IEEE Access
Multidisciplinary | Rapid Review | Open Access Journal

Received June 17, 2021, accepted July 9, 2021, date of publication July 13, 2021, date of current version July 22, 2021.

Digital Object Identifier 10.1109/ACCESS.2021.3097006

Optimal Power Flow Solution Based on Jellyfish Search Optimization Considering Uncertainty of Renewable Energy Sources

MOHAMED FARHAT[1], SALAH KAMEL[2], AHMED M. ATALLAH[1], AND BASEEM KHAN[3], (Member, IEEE)

[1]Electrical Power and Machines Engineering Department, Faculty of Engineering, Ain Shams University, Cairo 11517, Egypt
[2]Department of Electrical Engineering, Faculty of Engineering, Aswan University, Aswan 81542, Egypt
[3]Department of Electrical Engineering, Hawassa University, Hawassa 05, Ethiopia

Corresponding authors: Ahmed M. Atallah (atallah_eg@yahoo.com) and Baseem Khan (baseem.khan04@gmail.com)

This work was supported by the National Research and Development Agency of Chile (ANID) under Grant ANID/Fondap/15110019.

ABSTRACT Today's electrical power system became more complex interconnected network that is expanding every day. The transmission lines of the power system are more severely loaded than ever before. Hence, the power system is facing many problems such as power losses increasing, voltage instability, line overloads, etc. The optimization of real and reactive powers due to the installation of energy resources at appropriate buses can minimize the losses and improve the voltage profile especially, for congested networks. As a result, the optimal power flow problem (OPF) is considered more important tool for the processes of planning and operation of power systems. OPF is a very significant tool for power system operators to meet the electricity demand of the consumers efficiently, and for the reliable operation of the power system. However, the incorporation of renewable energy sources (RESs) into the electrical grid is a very challenging problem due to their intermittent nature. In this paper, the proposed power flow model contains three different types of energy sources: thermal power generators representing the conventional energy sources, wind power generators (WPGs), and solar photovoltaic generators (SPGs) representing RESs. Uncertain output powers from WPGs and SPGs are forecasted with the aid of Weibull and lognormal probability distribution functions (PDF), respectively. The under and overestimation output powers of RESs are taken into consideration while formulating the objective function through adding a penalty and reserve cost, respectively. Moreover, carbon tax is imposed to the main objective function to help in reducing carbon emissions. A jellyfish search optimizer (JS) is employed to reach optimization in the modified IEEE 30-bus test system to validate its feasibility. To examine the effectiveness of the proposed JS algorithm, its simulation results are compared with the results of four other nature-inspired global optimization algorithms. The developed OPF algorithm considers several practical cases such as generation uncertainty of renewable energy sources, time-varying load and the ramp rate limits of thermal generators. The simulation results show the effectiveness of the JS algorithm in solving the OPF problem in terms of minimization of total generation cost and solution convergence.

INDEX TERMS Optimal power flow, jellyfish search optimization, renewable energy resources, uncertainty.

NOMENCLATURE

List of abbreviation

ABC	Artificial bee colony
CGO	Chaos Game Optimization
GPC	Giza pyramids construction
FPA	Flower pollination algorithm
PDF	probability density function
ISO	Independent system operator
SF	Superiority of feasible solution
TG	Thermal generator
WPG	Wind power generator
SPG	Solar photovoltaic generator
RES	Renewable energy sources
a_i, b_i, c_i	Cost coefficients of the i -th thermal power generator

The associate editor coordinating the review of this manuscript and approving it for publication was Ehab Elsayed Elattar.

P_{TGi}	Output power of the i-th thermal generator
l_i and m_i	Valve-point loading effect coefficients
$P_{Ws,j}$	Scheduled wind power of the j-th wind power generator
d_j	Direct cost coefficient of the j-th wind power generator
$P_{Ss,k}$	Scheduled solar PV power of the k-th solar PV power plant
$K_{RW,j}$	Reserve cost coefficient of the j-th wind power plant
$P_{Wa,j}$	Available power from the j-th wind power plant
$K_{PW,j}$	Penalty cost coefficient of the j-th wind power plant
$K_{RS,k}$	Reserve cost coefficient of the k-th solar PV plant
$P_{Sa,k}$	Available power from the k-th solar PV power plant
P^0_{TGi}	Power of ith thermal generator at previous hour
$K_{PS,k}$	Penalty cost coefficient of the k-th solar PV power plant
C_{tax}	Carbon emission tax in \$/ton
C_E	Carbon emission cost in \$/h
$f_v(v)$	Probability of wind speed following Weibull PDF (m/s)
k, c	Weibull PDF shape and scale factors
$f_T(T)$	probability of solar irradiance (T) following lognormal PDF (W/m^2)
σ and μ	Standard deviation and mean of lognormal PDF
P_{loss}	Active power losses in the network
V_d	Voltage deviation
T	Solar irradiance (W/m^2)
DR_i, UR_i	down and up ramp-rate limits of i-th thermal power generator

I. INTRODUCTION

A. LITERATURE REVIEW

In 1962, optimal power flow (OPF) was first formulated by Carpentier [1]. Then several techniques for solving OPF have been proposed. OPF is employed for optimizing generation cost, reducing gas emissions, minimization of power losses, and keeping voltage stability. This optimization is usually forced by the physical limitations of the power system, where power generator capability, transmission line capacity, bus voltage, power cable flows, and any other technical constraints have to be satisfied. This can represent a fancy problem, especially in large power systems. Thus, distinctive care must be taken to guarantee that these technical constraints are not violated. Traditional OPF includes just conventional generation sources operating by firing fossil-fuel, and this already leads to an extremely non-linear, mixed integer, and non-convex optimization problem [2]–[5]. With high penetration levels of renewable energy sources (RES) in the power systems, OPF study becomes essential incorporating the uncertainty nature of these sources due to the associated challenges at the planning and operational phases. Since the initiation of OPF, many classical optimization methods have been proposed for solving OPF. These methods include interior-point methods, mixed-integer linear programming, non-linear programming, and quadratic programming [6]–[8].

Some of these methods have been successfully implemented by the industry sector because they have a fast convergence in addition to the strength in obtaining an optimum solution. However, such optimization methods require to linearizing the optimization function firstly. For this issue, some properties are often approximated for the optimization function like the non-convex, non-differentiable, and non-smooth properties.

To provide a solution for this problem, heuristic optimization techniques have also been suggested [9], [10]. In this regard, numerous heuristic techniques are used to solve the OPF.

Ref. [11], has presented a reliable and efficient Tabu search best method, which has been tested on the standard IEEE 30-bus power system, for achieving different objectives functions within several operating constraints.

Simulated annealing that is a single solution-based algorithm can provide a global or near global optimal solution but with high computational time [12].

In [13], a simple genetic algorithm (SGA) has been applied for solving OPF problem, where a sequential GA solution scheme has been employed to achieve suitable control variable resolution without violation of system constraints.

Ref. [14] has provided a hybrid genetic algorithm combining GA with the linear programming (LP) and sequential quadratic programming (SQP) algorithms available in the MATPOWER software.

Ref. [15] has presented a simple refined genetic algorithm (RGA) with the ability to code large number of control variables in a practical power system, within a reasonable length of chromosome.

In [16], a multi-parent crossover based genetic algorithm (GA-MPC) has been presented to solve OPF problem of power system consisting of thermal generators considering various objective functions such as piecewise quadratic cost, total fuel cost, valve-point loading effects and emission.

In [17], an enhanced genetic algorithm has been presented for solving OPF problem. This algorithm has been validated using IEEE 30-bus power system and the three area IEEE RTS-96.

Differential evolution (DE) has been applied to solve OPF problem in many previous works. It is suitable for OPF problems including complex variables or transient stability constraints and it has fast convergence characteristics but the probability of converging to a local, rather than global, optima is high [18]–[22].

Particle swarm optimization (PSO) has been used in several difficult OPF problems. However, as with many heuristic

approaches, a primary drawback of traditional PSO is premature convergence when the parameters are not chosen correctly [23]–[28].

In recent years, many meta-heuristic population based algorithms are used for solving OPF problems such as artificial bee colony (ABoC) [29], grey wolf optimization (GWO) [30], flower pollination algorithm (FPA) [31], crow search algorithms (CSA) [32], group search optimization (GSO) [33], cuckoo search optimization (CSO) [34], moth swarm algorithm (MSA) [35], bacterial foraging algorithm (BFA) [36], success history-based adaptive differential evolution (SHADE) algorithms [37], and JAYA algorithm [38], [39]. In literature, different modifications have been done on the heuristic optimization techniques to overcome the problem of premature convergence and get a better solution of the OPF problem with RES and different objective functions.

In [36], authors provided a modified bacteria foraging algorithm (MBFA) to solve OPF incorporating with a model for doubly fed induction generator (DFIG), thermal power generators and static synchronous compensator (STATCOM).

The authors in Ref. [40] have proposed a new modification on JAYA algorithm (MJAYA) to provide a solution for the premature convergence problem of the original JAYA.

Ref. [41] proposed a global best artificial bee colony algorithm, not only to improve the initialization phase of ABC algorithm, but to enhance the search technique to reach an optimum solution as well.

Ref. [37] proposed a modification on DE called SHADE algorithm where the selection process of future control parameters is guided through the successful control parameters settings to guarantee an appropriate balance concerning the exploration and exploitation phases. Moreover, this helped in achieving comparatively fast convergence rate for OPF problems.

Ref. [42] proposed a combination between SHADE and a technique for handling constraints, called the superiority of feasible solution (SF) which helped in increasing the efficiency of SHADE.

B. CONTRIBUTION AND PAPER ORGANIZATION

This paper comes in the context of completing the exerted efforts to find an optimal solution for the OPF problem. In this paper, a new recent metaheuristic optimization algorithm called jellyfish search (JS) which is developed in [43] is used to efficiently solve the OPF problem. The proposed algorithm is applied to IEEE 30 –bus system incorporating with two wind generators and one solar PV generator to verify its validity in obtaining the optimal solution for OPF problem with renewable energy sources during theoretical and practical conditions. Four other optimization techniques: Giza pyramids construction (GPC) [44], chaos game optimization (CGO) [45], flower pollination algorithm (FPA) [46] and artificial bee colony (ABC) [29] are applied to the proposed system to compare their results with the results of JS. The results of JS are also compared with the results obtained by SHADE-SF in [42].

The structure of the rest of this paper is prepared as follows. Section II shows the mathematical model and associated applicable constraints applied for the OPF problem. Section III introduces the uncertainty output models of WPG and SPG. In section IV, the new proposal for applying JS to OPF including the uncertain RES is developed. Section V provides simulation results of numerous realistic case studies for the five algorithms under study. Finally, section VI presents conclusions for this paper.

II. PROBLEM FORMULATION

Table 1 summarizes the parameters of IEEE 30-bus system under work. The modified network involves three different types of power generation resources i.e. thermal power generators (TGs) with constant outputs, solar PV generator (SPG) with variable output, and wind generators (WPG) with variable outputs. This variation in PV and wind outputs must be balanced through the mixture of all generators and reserve power, so the overall generation cost comprises costs of operation for all generators, reserve cost and penalty cost.

A. COST MODEL FOR THERMAL POWER GENERATORS

Thermal power generators use the fossil fuel to operate. The relation between the fossil fuel cost in \$/hr and thermal generator output power in MW is given by (1).

$$C_{T0}(P_{TG}) = \sum_{i=1}^{N_{TG}} a_i + b_i P_{TGi} + c_i P_{TGi}^2 \tag{1}$$

where a_i, b_i, c_i represent the cost coefficients of the i -th thermal power generator with power output P_{TGi}. N_{TG} is the total number of thermal power generators.

However, taking the valve point loading effect in our consideration gives more precise and realistic cost, so the modified quadratic relationship with a valve point loading effect will be as following:

$$C_T(P_{TG}) = \sum_{i=1}^{N_{TG}} a_i + b_i P_{TGi} + c_i P_{TGi}^2 + \left| l_i * sin(m_i * (P_{TGi}^{min} - P_{TGi})) \right| \tag{2}$$

where, l_i and m_i represent coefficients of the valve-point loading effect. P_{TGi}^{min} is the minimum power of i-th thermal unit generator.

Table 2 provides all cost and emission coefficients used in calculations related to the thermal generating units.

B. DIRECT COST OF POWER PRODUCED FROM WIND AND SOLAR PHOTOVOLTAIC SOURCES

WPGs and SPG do not need fossil fuel to operate. They depend on wind and the sun to generate power.

When an independent system operator (ISO) owns the solar PV/wind generators, the cost function might not be as the solar PV/wind generators need no fuel, unless ISO desires to allocate some reimbursement cost to the initial expenditure

TABLE 1. IEEE-30 bus system characteristics [42].

Items	Quantity	Details
Buses	30	[47]
Branches	41	[47]
Thermal generators (TG1, TG2, TG3)	3	Buses: 1 (swing), 2 and 8
Wind power generators (WPG1,WPG2)	2	Buses: 5 and 11
Solar PV generator (SPG)	1	Bus: 13
Control variables	11	Scheduled real power for 5 Nos. generators: TG2, TG3, WPG1, WPG2 and SPG, voltages of generator buses (6 Nos.)
Connected load	-	283.4 MW, 126.2 MVAr
Allowed range for voltage of load buses	24	[0.95–1.05] p.u.

TABLE 2. Coefficients of emission and cost for thermal power generators in the system under study [48].

Gen.	Bus	a	b	c	l	m	α	β	γ	ω	μ	P^0_{TGi} (MW)	DR_i (MW)	UR_i (MW)
TG1	1	0	2	0.00375	18	0.037	4.091	-5.554	6.49	0.0002	6.667	99.211	20	15
TG2	2	0	1.75	0.0175	16	0.038	2.543	-6.047	5.638	0.0005	3.333	80	15	10
TG3	8	0	3.25	0.00834	12	0.045	5.326	- 3.55	3.38	0.002	2	20	8	4

for these plants or to allocate this in a form of the cost required for maintenance and renewal [42]. On another side, when private parties own solar PV or wind generators, ISO is obliged to pay a price in proportion to the scheduled power contracted.

The direct cost of the j-th wind power generator as a function of scheduled power is molded as following,

$$C_{Wd,j} = d_j P_{Ws,j} \tag{3}$$

where $P_{Ws,j}$ and d_j are the scheduled wind power and the direct cost coefficient related to the j-th wind power plant respectively.

In a same way, the direct cost of the k-th solar PV power generator is:

$$C_{Sd,k} = e_k P_{Ss,k} \tag{4}$$

where $P_{Ss,k}$ and e_k are the scheduled solar PV power and the direct cost coefficient related to the k-th solar PV power plant respectively.

C. EVALUATION OF COST DUE TO UNCERTAINTIES IN WIND POWER

There are two scenarios may occur due to the intermittent nature of wind energy. The first scenario takes place when the output power of the wind plant is less than the expected output power. This situation is termed as overestimation of output power. In this situation, the system operator uses spinning reserve to provide reliable power supply to its consumers.

The cost required for committing the reserve generating units to overcome the overestimation situation is referred to reserve cost.

Reserve cost for the j-th wind power plant is determined by:

$$\begin{aligned} &C_{Wr,j}(P_{Ws,j} - P_{Wa,j}) \\ &\quad = K_{RW,j}(P_{Ws,j} - P_{Wa,j}) \\ &\quad = K_{RW,j}\int_0^{P_{Ws,j}} (P_{Ws,j} - P_{W,j}) f_W(P_{W,j}) dP_{W,j} \end{aligned} \tag{5}$$

where $K_{RW,j}$ and $P_{Wa,j}$ are the reserve cost coefficient and the available power relating to the j-th wind power plant respectively, and $f_W(P_{W,j})$ is referred as the PDF for the output power of the j-th wind power farm.

The second scenario occurs when the output power of the wind power plant is higher than the anticipated value of the output power. This situation is expressed as underestimation of output power. Consequently, the remaining power will be lost if it is not possible to consume through decreasing the output power of conventional generators. In this situation ISO has to compensate a penalty cost associated to the remaining power.

Penalty cost of wind power farm j is determined by:

$$\begin{aligned} &C_{Wp,j}(P_{Wa,j} - P_{Ws,j}) \\ &\quad = K_{PW,j}(P_{Wa,j} - P_{Ws,j}) \\ &\quad = K_{PW,j}\int_{P_{Ws,j}}^{P_{Wr,j}} (P_{W,j} - P_{Ws,j}) f_W(P_{W,j}) dP_{W,j} \end{aligned} \tag{6}$$

where $K_{PW,j}$ and $P_{Wr,j}$ are the penalty cost coefficient and the rated power relating to the j-th wind power plant respectively.

D. EVALUATION OF COST DUE TO UNCERTAINTIES IN SOLAR PHOTOVOLTAIC POWER

Similar to wind energy, solar energy has also uncertain and intermittent output. The approach used to solve under and overestimation of solar output power should be in principle the same as the wind output power.

However, for more simplicity in calculations, penalty and reserve cost models are formed following the proposed concept in Ref. [49].

This concept is used because solar radiation follows log-normal PDF [50], which represents a meaningful difference comparing to the Weibull PDF used for wind speed distribution.

More details are provided in Section III for calculating stochastic solar PV and wind power.

The reserve cost of solar PV power plant k is given by:

$$\begin{aligned} &C_{Sr,k}(P_{Ss,k} - P_{Sa,k}) \\ &\quad = K_{RS,k}(P_{Ss,k} - P_{Sa,k}) \\ &\quad = K_{RS,k} * f_s(P_{Sa,k} < P_{Ss,k}) * [(P_{Ss,k} - E(P_{Sa,k} < P_{Ss,k})] \end{aligned} \tag{7}$$

where $K_{RS,k}$ represents the coefficient of reserve cost and $P_{Sa,k}$ is the available power related to solar PV power plant k. $f_s(P_{Sa,k} < P_{Ss,k})$ represents the solar power shortage probability, while $E(P_{Sa,k} < P_{Ss,k})$ referrers to the expected output of the solar PV power generator below $P_{Ss,k}$.

The penalty cost of solar PV power generator k is given by:

$$\begin{aligned} &C_{Sp,k}(P_{Sa,k} - P_{Ss,k}) \\ &\quad = K_{PS,k}(P_{Sa,k} - P_{Ss,k}) \\ &\quad = K_{PS,k} * f_s(P_{Sa,k} > P_{Ss,k}) * [(E(P_{Sa,k} < P_{Ss,k}) - P_{Ss,k}] \end{aligned} \tag{8}$$

where $K_{PS,k}$ is the penalty cost and $f_s(P_{Sa,k} > P_{Ss,k})$ represents the probability of remaining power generated by the solar PV power plant k comparing to $P_{Ss,k}$, while $E(P_{Sa,k} < P_{Ss,k})$ referrers to the expected remaining output power.

E. CARBON EMISSIONS AND TAX

Using conventional energy sources to produce power is well known as a source of emitting greenhouse gases into the environment. Two of these harmful gases are SO_x and NO_x which increase in emitting with growth in produced power from conventional power generators. The relationship between emission in tonnes per hour (t/h) and produced power (in p.u. MW) is represented through Eq. (9).

$$\mathrm{E} = \sum_{i=1}^{N_{TG}} [(\alpha_i + \beta_i P_{TGi} + \gamma_i P_{TGi}^2) * 0.01 + \omega_i e^{(\mu_i P_{TGi})}] \tag{9}$$

where α_i, β_i, γ_i, ω_i and μ_i represent emission coefficients associated to the thermal power generator i.

Values of emission coefficients related to the thermal power generator are illustrated in Table 2. Which are similar to values mentioned in [48] with some slight change in the value of μ for the thermal power generator linked to bus 1.

In current years, owing to the harmful impact of climate change, energy regulators in several countries are setting huge regulations on the whole energy industry sector to decrease the carbon emission [51]. To encourage investors to invest in clean and renewable energy sources like solar and wind, carbon tax (C_{tax}) is enforced per ton of greenhouse gasses. The cost of carbon emission in \$/h is calculated as:

$$C_E = C_{tax} E \tag{10}$$

F. OBJECTIVE FUNCTIONS

The objective optimization for OPF is formed including all models of cost functions as illustrated in Eqs. 2-8.

In objective function (F1), emission cost is neglected. To clarify the variation in the scheduling of generation when considering a carbon tax, the objective function (F2) is formulated including emission cost as illustrated in Eqs.9-10.

Consequently, the first objective function is to minimize:

$$\begin{aligned} F1 = C_T(P_{TG}) + \sum_{j=1}^{N_{WG}} [d_j P_{Ws,j} + K_{RW,j}(P_{Ws,j} - P_{Wa,j}) \\ + K_{PW,j}(P_{Wa,j} - P_{Ws,j})] + \sum_{j=1}^{N_{SG}} e_k P_{Ss,k} \\ + K_{RS,k}(P_{Ss,k} - P_{Sa,k}) + K_{PS,k}(P_{Sa,k} - P_{Ss,k})] \end{aligned} \tag{11}$$

where, N_{WG} and N_{SG} represent the number of wind power generators and solar PV generators existing in the system respectively.

The second objective function is to minimize:

$$F2 = F1 + C_{tax} E \tag{12}$$

The above-mentioned OPF objective functions are exposed to both inequality and equality constraints of the system as illustrated below.

1) EQUALITY CONSTRAINTS

Equality constraints are necessary load flow equations for providing power balance of both active and reactive powers generated in the system. This mean that these powers must be equal to the total demand and total losses in the system. The equality constraints are represented as follows [42]:

$$P_{Gi} = P_{Di} + V_i \sum_{i=1}^{NB} V_j [G_{ij} cos(\delta_{ij}) + B_{ij} sin(\delta_{ij})] \quad \forall\, i \in NB \tag{13}$$

$$Q_{Gi} = Q_{Di} + V_i \sum_{i=1}^{NB} V_j [G_{ij} sin(\delta_{ij}) - B_{ij} cos(\delta_{ij})] \quad \forall\, i \in NB \tag{14}$$

where $\delta_{ij} = (\delta_{i-}\delta_j)$ is the voltage angles difference between buses i and j, NB refers to the total number of network buses, P_{Di} and Q_{Di} represent active and reactive components of load demand connected to bus i respectively whilst the active and reactive power components of generation at bus i are represented by P_{Gi} and Q_{Gi} respectively from any of the energy resources either conventional power plants or renewable energy plants. G_{ij} and B_{ij} are the transfer conductance and susceptance is between buses i and j respectively.

2) INEQUALITY CONSTRAINTS

The inequality constraints represent the operating limits of components and equipment in power system. These constraints include also security constraints on transmission lines and load buses.

(a) Generator's constraints:

$$P_{TGi}^{min} \le P_{TGi} \le P_{TGi}^{max}, \quad i = 1, \ldots\ldots\ldots, N_{TG} \tag{15}$$
$$P_{Ws,j}^{min} \le P_{Ws,j} \le P_{Ws,j}^{max}, \quad j = 1, \ldots\ldots\ldots, N_{WG} \tag{16}$$
$$P_{Ss,k}^{min} \le P_{Ss,k} \le P_{Ss,k}^{max}, \quad k = 1, \ldots\ldots\ldots, N_{SG} \tag{17}$$
$$Q_{TGi}^{min} \le Q_{TGi} \le Q_{TGi}^{max}, \quad i = 1, \ldots\ldots\ldots, N_{TG} \tag{18}$$
$$Q_{Ws,j}^{min} \le Q_{Ws,j} \le Q_{Ws,j}^{max}, \quad j = 1, \ldots\ldots\ldots, N_{WG} \tag{19}$$
$$Q_{Ss,k}^{min} \le Q_{Ss,k} \le Q_{Ss,k}^{max}, \quad k = 1, \ldots\ldots\ldots, N_{SG} \tag{20}$$
$$V_{Gi}^{min} \le V_{Gi} \le V_{Gi}^{max}, \quad i = 1, \ldots\ldots\ldots, N_{G} \tag{21}$$

(b) Security constraints:

$$V_{L_p}^{min} \le V_{L_p} \le V_{L_p}^{max}, \quad p = 1, \ldots\ldots\ldots, N_L \tag{22}$$
$$S_{L_q} \le S_{L_q}^{max}, \quad q = 1, \ldots\ldots\ldots, N_L \tag{23}$$

The generation limits of active power for thermal generators, wind generators, and solar PV generators are represented by Eqs. (15) – (17) respectively. With the same arrangement, Eqs. From (18) to (20) represent reactive power limits of all generators. While N_G represents the total number of generator buses or generators. Eq. (21) defines constraints on generator buses voltage, and Eq. (22) provides voltage limits subjected to PQ buses (load buses) and N_L refers to the number of PQ buses. Eq. (23) defines the constraints on the transmission Lines capacity for total N_L numbers of transmission lines within the system.

It is important to note that power flow convergence to an optimal solution guarantees automatically satisfying the imposed equality constraints through equations of power balance. Amongst inequality constraints, voltages of generator buses and active powers of generators (excluding swing or slack generator assumed to be linked to bus 1) are characterized as self-limiting control variables.

For each variable from the control variables, the applied optimization technique chooses a reasonable value lied in the accepted range of this variable. Thus, inequality constraints related to the active and reactive power outputs of the slack generator, reactive power outputs of other generators, PQ buses' voltage limits, and transmission line capabilities require special attention.

3) PRACTICAL CONSTRAINTS

Thermal power generators are regulated to operate always between two adjacent limits.

Generally, thermal power generators are connected with steam valves to decrease or increase their power generation. In real- time, due to physical limitations, the power generated from a thermal generator tracks ramp-functions i.e. to decrease the produced power, the generator follows down ramp-rate, and to increase the produced power, the generator follows up ramp-rate. The ramp rate limits can be mathematically formed as:

$$max(P_{TGi}^{min}, P_{TGi}^{0} - DR_i) \le P_{TGi} \le, \quad min(P_{TGi}^{max}, P_{TGi}^{0} + UR_i), \times i = 1, \ldots\ldots\ldots, N_{TG} \tag{24}$$

where, P_{TGi}^{0} represents the ith generator power generation at previous hour. DR_i and UR_i represent the respective down and up ramp-rate limits of i-th thermal power generator, respectively.

The ramp-rate constraints can be given in OPF problem as follows:

$$P_{TGi}^{0} - P_{TGi} \le DR_i, \quad if\ generation\ decreases$$
$$P_{TGi} - P_{TGi}^{0} \le UR_i, \quad if\ generation\ increases$$

In OPF problem, due to the existence of ramp-rate limits, the generation fuel cost increases because the operating points of the thermal generating units are changed from its operating limits. The new upper and lower limits of a thermal generator considering ramp-rate limits must not exceed the following limits:

$$P_{TGi}^{high} = min(P_{TGi}^{max}, P_{TGi}^{0} + UR_i) \tag{25}$$
$$P_{TGi}^{low} = max(P_{TGi}^{min}, P_{TGi}^{0} - DR_i) \tag{26}$$

P_{TGi}^{high} and P_{TGi}^{low} are the new limits of thermal unit-i.

G. LOAD BUS MODELLING

The reactive power capability of the generator is a vital issue in the OPF study. In this work, narrower ranges are applied for thermal power generators than what have been applied in [47]. In recent years, the reactive power capability of wind power plants has significantly developed. Commercially, wind turbines (WTs) including full reactive power capability and other important features are already available [52].

With the assistance of the Enercon FACTS – WT reactive capability curve, it is clear that a wind turbine can deliver reactive power from −0.4 p.u. to 0.5 p.u. throughout its range of output active power. Delivering negative reactive power indicates the capability of the generator to absorb reactive power.

A rooftop solar PV system can be characterized as PQ bus (load bus) with reactive power equal to zero (Q = 0). While large scale solar PV systems are connected with inverters. As a result, a full capability model of solar PV generator is necessary due to the dynamic performance of the inverters [53].

In this aspect, ref. [54] provides converter and controller models when implementing a detailed study of reactive power capabilities of solar PV generator. In ref. [55], the PV converter capability study has been extended taking into consideration the impact of change in solar irradiance and surrounding temperature. In this work, the reactive power capability chart of solar PV generator is nearly considered from −0.4 p.u. to 0.5 p.u.

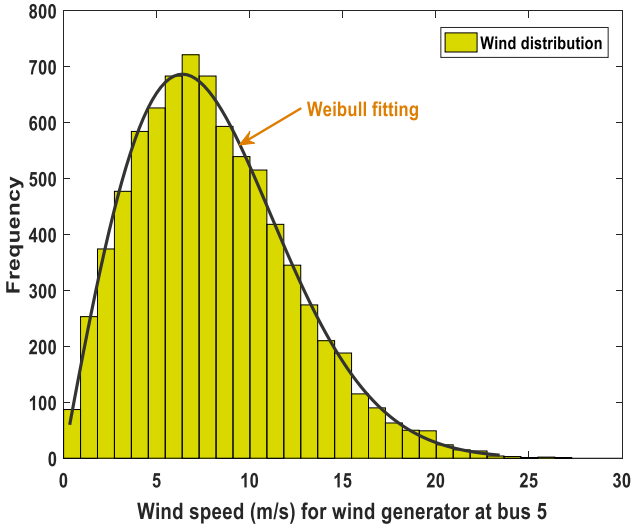

FIGURE 1. Distribution of wind speed for wind power generator 1 at bus 5 (c = 9, k = 2).

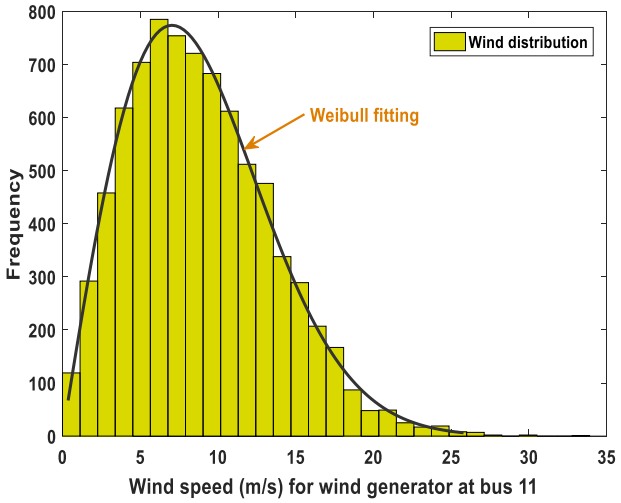

FIGURE 2. Distribution of wind speed for wind power generator 2 at bus 11(c = 10, k = 2).

All limits of active and reactive powers of the power generators in the system under study are illustrated in Table 5 in addition to simulation results.

Parameters of the system like voltage deviation and active power loss in the transmission lines are also important in OPF problem study. The active power loss in transmission lines is unavoidable due to the inherent resistance of the lines. The real power loss of the network is calculated by:

$$P_{loss} = \sum_{i=1}^{NL} \sum_{j\neq 1}^{NL} G_{ij} V_i^2 + V_j^2 - 2V_i V_j \cos(\delta_{ij}) \quad (27)$$

where δ_{ij} represents the difference of voltage angles between buses i and j and G_{ij} refers to the transfer conductance.

The voltage deviation indicator represents the cumulative deviation of voltages of all PQ buses (load buses) in the system from a nominal value (1 p.u.). It provides an indicator for the quality of power system voltage and mathematically expressed as:

$$V_d = \sum_{p=1}^{NL} |V_{Lp} - 1| \quad (28)$$

III. STOCHASTIC WIND POWER, SOLAR POWER AND UNCERTAINTY MODELS

Refs. [36] and [49] show that wind speed distribution follows Weibull probability density function (PDF) for mean power calculations of wind turbines. The probability of wind speed according Weibull PDF is given by:

$$f_v(v) = \left(\frac{k}{c}\right) + \left(\frac{v}{c}\right)^{(k-1)} e^{-(v/c)^k} \quad for\ 0 < v < \infty \quad (29)$$

where v is wind speed in m/s, k is the shape factor and c is scale factor.

Eq. 30 defines the mean of Weibull distribution:

$$M_{wbl} = c * \Gamma(1 + k^{-1}) \quad (30)$$

where Γ is gamma function that is defined as:

$$\Gamma(x) = \int_0^{\infty} e^{-t} t^{x-1} dt \quad (31)$$

The IEEE-30 bus system is adjusted in this study by replacing conventional generators connected to buses 5 and 11 with two wind power plants. Table 3 provides the selected values of Weibull scale (c) and shape (k) parameters. These values have been followed in this study except other values used for a specific case study. Figs. 1 and 2 provide Weibull fitting and distributions of wind frequency. They are got after running Monte Carlo simulation with 8000 iterations [42]. Ref. [56] regulates the requirement of wind turbine design and states the maximum turbulent class IA of the wind turbine which is suitable for operation at the maximum annual average wind speed (10 m/s at hub height). Shape (k) and scale (c) parameters for the wind farms are carefully selected to remain the maximum value of Weibull mean around 10 to guarantee both realistic and diverse geographic locations for the two wind farms.

In the same way, we replaced the conventional generator connected to bus 13 of the IEEE-30 bus system with solar PV generator. The output of solar PV generator depends on the solar irradiance (T) which follows lognormal PDF [50]. The probability of solar irradiance (T) following lognormal PDF is given by:

$$f_T(T) = \frac{1}{T\sigma\sqrt{2\pi}} exp\left\{\frac{-(lnx - \mu)^2}{2\sigma^2}\right\} \quad for\ T > 0 \quad (32)$$

where σ and μ are the standard deviation and mean of lognormal PDF respectively.

$$M_{lgn} = exp(\mu + \frac{\sigma^2}{2}) \quad (33)$$

Fig. 3 shows lognormal PDF of solar irradiance after Monte Carlo simulation with 8000 iterations.

TABLE 3. Parameters of PDF for wind and solar PV plants.

Wind power plants					Solar PV plant		
Wind plant #	No. of Turbines	Rated power, P_{Wr} (MW)	Weibull PDF Parameters	Weibull mean, M_{wbl}	Rated power, P_{Sr} (MW)	Lognormal PDF parameters	Lognormal mean, M_{lgn}
1 (bus 5)	25	75	c=9, k=2	v = 7.976 m/s	50 (bus 13)	μ=6, δ=0.6	T=483W/m^2
2 (bus 11)	20	60	c=10, k=2	v = 8.862 m/s			

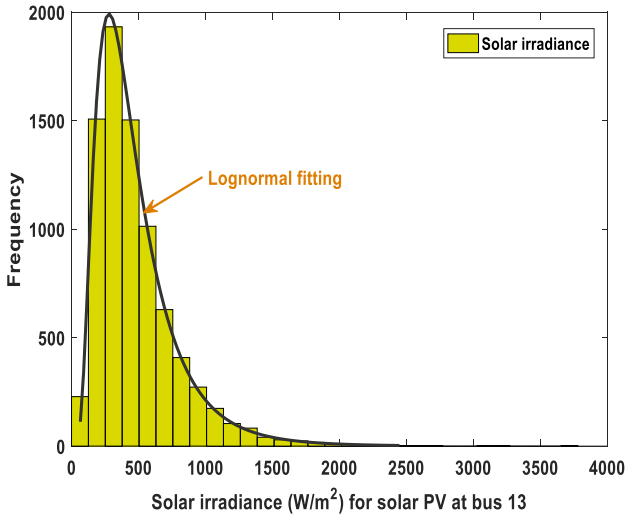

FIGURE 3. Distribution of solar irradiance for solar PV generator at bus 13 ($\mu = 6$, $\sigma = 0.6$).

Table 3 provides the chosen values for lognormal PDF parameters. These values have been followed in this study except other values used for a specific case study.

A. WIND POWER AND SOLAR PHOTOVOLTAIC POWER MODELS

As mentioned above, the modified IEEE-30 bus system has two wind power farms. Wind farm 1 is connected to bus 5, it consists of 25 wind turbines with a rated power of 3 MW for each turbine, and thus the cumulative active power of wind farm 1 is 75 MW. Similarly, wind farm 2 is connected to bus 11, it contains 20 wind turbines, and each turbine has a rated power of 3 MW, thus the cumulative active power of wind farm 2 is 60 MW.

The actual output power of wind power generator depends on the wind speed. A wind turbine output power is given by [42]:

$$P_W(v) = \begin{cases} 0, & for\ v < v_{in}\ and\ v > v_{out} \\ P_{Wr}\left(\dfrac{(v - v_{in}}{(v_r - v_{in}}\right) & for\ v_{in} \le v \le v_r \\ P_{Wr} & for\ v_r \le v \le v_{out} \end{cases} \quad (34)$$

where v_r, v_{out}, and v_{in} are the rated, cut-out, and cut-in wind speeds of the wind power turbine respectively. P_{wr} represents the rated output power of the wind turbine. Based on the product datasheet of Enercon E82-E4 wind turbine, various speeds of a 3-MW wind turbine are v_r s = 16, m/s v_{out} = 25 m/s, and v_{in} = 3 m/s.

Similarly, the energy conversion for solar PV in terms of solar irradiance (T) is expressed by [57]:

$$P_S(T) = \begin{cases} P_{Sr}\left(\dfrac{T^2}{T_{std}R_c}\right) & for\ 0 < T < R_c \\ P_{Sr}\left(\dfrac{T}{T_{std}}\right) & for\ T \ge R_c \end{cases} \quad (35)$$

where T_{std} is the solar irradiance set as 800 W/m^2. in standard environment, R_c represents a certain irradiance point fixed as 120 W/m^2. and P_{Sr} is the rated output power of the solar PV unit.

B. WIND POWER PROBABILITY MODEL

Based on (34), the variable output power of wind generators is discrete in some regions of wind speed. The output power is zero when wind speed (v) is lower than cut-in speed (v_{in}) and higher than cut-out speed (v_{out}), while the output power will be at its rated value P_{wr} when the wind speed lies between rated wind speed (v_r) and cut-out speed (v_{out}). The wind output power probabilities for these discrete zones are described by [58]:

$$f_W(P_W)\{P_W = 0\} = 1 - \exp\left[-\left(\frac{v_{in}}{c}\right)^k\right] + \exp\left[-\left(\frac{v_{out}}{c}\right)^k\right] \quad (36)$$

$$f_W(P_W)\{P_W = P_{Wr}\} = \exp\left[-\left(\frac{v_r}{c}\right)^k\right] - \exp\left[-\left(\frac{v_{out}}{c}\right)^k\right] \quad (37)$$

The output power of wind turbine is continuous between cut-in speed (v_{in}) and rated speed (v_r) of wind. The probability of wind output power in the continuous zone are described by [13]:

$$f_W(P_W) = \frac{k(v_r - v_{in})}{c^k * P_{Wr}}\left[v_{in} + \frac{P_W}{P_{Wr}}(v_r - v_{in})\right]^{k-1} * \exp\left[-\left(\frac{v_{in} + \frac{P_W}{P_{Wr}}(v_r - v_{in})}{c}\right)^k\right] \quad (38)$$

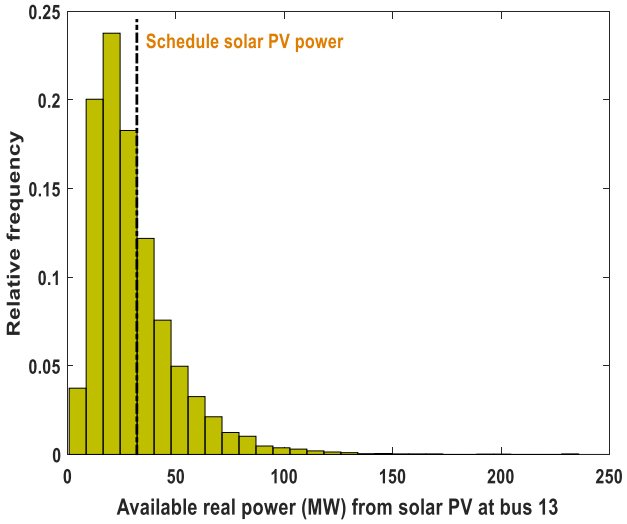

FIGURE 4. Distribution of real power (MW) for solar PV generator at bus 13.

C. SOLAR PV POWER OVER/UNDERESTIMATION COST

The stochastic output power from the solar PV plant is represented by the histogram in Fig. 4. The dotted line illustrates the scheduled power supposed to be delivered to the network by the solar PV generator. It is necessary to observe that scheduled solar PV power is a variable value, so there is a jointly power agreement between the ISO and the owner of the solar PV generator. Eqs. (39) and (40) are used in the model to calculate over and underestimation cost of the solar PV generator respectively:

$$C_{Sr,k}\,(P_{Ss} - P_{Sa}) = K_{RS}\,(P_{Ss} - P_{Sa}) = K_{RS}\sum_{n=1}^{N^-}[P_{Ss} - P_{Sn-}] * f_{Sn-} \quad (39)$$

$$C_{Sp,k}\,(P_{Sav} - P_{Ss}) = K_{PS}\,(P_{Sa} - P_{Ss}) = K_{PS}\sum_{n=1}^{N^+}[P_{Sn+} - P_{Ss}] * f_{Sn+} \quad (40)$$

where P_{Sn-} and P_{Sn+} are the shortage power and surplus power, as lying on the right and left half plane of schedule power P_{Ss} in the histogram of Fig. 4. Likewise, f_{Sn-} and f_{Sn+} are relative frequencies for the occurrence of P_{Sn-} and P_{Sn+}. N^- and N^+ represent number of discrete bins on the left and right planes of P_{Ss} for PDF generation.

IV. OPTIMISATION TECHNIQUE

In 2020, a novel metaheuristic optimizer titled artificial jellyfish search optimizer has been proposed by J.-S. Chou and D.-N. Truong [43]. The behavior of jellyfish for finding food in the ocean inspired the JS algorithm. At the beginning, they follow ocean current, then they move inside swarms as time passes on, in the presence of a mechanism to control the time of switching amongst these motions.

A. MATHEMATICAL MODEL

The proposed optimization technique depending on three main rules.

1. Jellyfish either pursue the ocean currents or proceed inside swarms, and a time control mechanism regulates the switching process between these motions.
2. Jellyfish proceed in the ocean seeking food. They are highly attracted to places that have a greater amount of food.
3. The amount of food found by jellyfish is determined through the position and its correspondent objective function.

1) CURRENT OF OCEAN

The ocean current includes huge quantities of nutrients that attract jellyfish. Eq. (41) determines the ocean current direction through taking the average of the entirely vectors from every jellyfish in the ocean to that is presently in the best position.

$$Trend^{\rightarrow} = \frac{1}{N_{Pop}}\sum Trend_i^{\rightarrow} = \frac{1}{N_{Pop}}\sum (X^* - e_c X_i) = X^* - e_c\frac{\sum X_i}{N_{Pop}} = X^* - e_c\mu_s \quad (41)$$

Set

$$df = e_c\mu_s \quad (42)$$

Therefore $trend^{\rightarrow}$ is determined by:

$$Trend^{\rightarrow} = X^* - df \quad (43)$$

where N_{Pop} represents jellyfish number, X^* represents the jellyfish presently in the best position in the jellyfish swarm, while e_c refers to the control factor that manages the attraction process, the mean position of whole jellyfish in the ocean is represented by μ_s, df refers to the difference between the current best position of the jellyfish and the mean position of all jellyfish.

Assume that jellyfish distribute with a normal spatial distribution in all dimensions, thus there will be a distance $(\pm\beta_s\sigma_s)$ nearby the mean position includes a certain probability of all jellyfish.

where σ_s refers to the standard deviation of the normal spatial distribution.

Therefore,

$$df = \beta_s * \sigma_s * rand^f(0, 1) \quad (44)$$

Set

$$\sigma_s = rand^{\alpha_s}(0, 1) * \mu_s \quad (45)$$

Hence,

$$df = \beta_s * rand^f(0, 1) * rand^{\alpha_s}(0, 1) * \mu_s \quad (46)$$

To make it simpler, Eq. 43 is formed as follows:

$$df = \beta_s * \mu_s * rand(0, 1) \quad (47)$$

where

$$e_c = \beta_s * rand(0, 1) \tag{48}$$

Thus,

$$Trend^{\rightarrow} = X^* - \beta_s * rand(0, 1) * \mu_s \tag{49}$$

So, we can define the new position of each jellyfish by:

$$X_i(t + 1) = X_i(t) + rand(0, 1) * Trend^{\rightarrow} \tag{50}$$

Eq. 47 can be written as:

$$X_i(t + 1) = X_i(t) + rand(0, 1) * X^* - \beta_s * rand(0, 1) * \mu_s \tag{51}$$

where $\beta_s > 0$ refers to the distribution coefficient, associated with the $Trend^{\rightarrow}$ length. In this case, β_s =3.

2) SWARM OF JELLYFISH

In a swarm, there are two types of motions: type A (passive motion) and type B (active motion). In the beginning, when the jellyfish swarm has just been shaped, most of jellyfish show passive motion. As time passes on, they increasingly show active motion. In passive motion, jellyfish move around their original locations. Consequently, each jellyfish updates its location by (52).

$$X_i(t + 1) = X_i(t) + \gamma_s * rand(0, 1) * (U_B - L_B) \tag{52}$$

where U_B and L_B represent the upper and lower bounds of the search space, respectively. $\gamma_s > 0$ represents the motion coefficient, associated with the motion length around locations of jellyfish. In this paper, $\gamma_s = 0.1$.

To simulate the active motion (type B), we will randomly select a jellyfish (Jf_j) different to the jellyfish of interest (Jf_i). Consequently, to determine the direction of motion, a vector from Jf_i to the Jf_j is utilized to define the direction of motion. When the amount of food founded at the position of Jf_j is greater than the amount at the position of Jf_i, Jf_i moves in the direction of Jf_j. In contrast, if the available amount of food to Jf_j is lesser than the available amount to Jf_i, Jf_i moves directly in opposite direction of Jf_j. Thus, each jellyfish in a swarm moves directly to the better trend to find food. The motion direction and the updated location of a jellyfish are simulated by (55) and (56), respectively. This movement represents an effective way to exploit the search space.

$$Step^{\rightarrow} = X_i(t + 1) - X_i(t) \tag{53}$$

where

$$Step^{\rightarrow} = rand(0, 1) * Direction^{\rightarrow} \tag{54}$$

$$Direction^{\rightarrow} = \begin{cases} X_j(t) - X_i(t) & if\ f(X_i) \geq f(X_j) \\ X_i(t) - X_j(t) & if\ f(X_i) < f(X_j) \end{cases} \tag{55}$$

where, $f(X)$ represents the objective function and X represents the location of jellyfish.

Therefore,

$$X_i(t + 1) = X_i(t) + Step^{\rightarrow} \tag{56}$$

A mechanism for time control is set to define the motion type over time. Its function is to control not only passive and active motions in a jellyfish swarm but also the movements in the direction of the ocean current.

3) MECHANISM OF TIME CONTROL

Ocean currents contain large quantities of food that attract jellyfish. As time passes on, a swarm of jellyfish is formed through gathering more jellyfish together. When the ocean current changes by wind or temperature, the jellyfish existing in the formed swarm move in the direction of another suitable ocean current and consequently another swarm of jellyfish is formed.

As mentioned above, there are two types of jellyfish motion inside a swarm: passive motions (type A) and active motion (type B), the motion of jellyfish is switched between them. In the beginning, jellyfish prefer the motion of type A; as time passes on, the motion of type B is favored.

The mechanism of time control is presented to provide a simulation for this situation. The time control mechanism regulates the switching process between the two types of motion by determining the time control function C(t) represented by (57). The value of C(t) fluctuates from 0 to 1 overtime. This value is compared with a constant C_o., when it is greater than C_o, the jellyfish follow the ocean current. When its value is lower than C_o, jellyfish tend to move inside the swarm. The value of C_o is assumed to 0.5.

$$C(t) = \left| \left(1 - \frac{t}{Max_{iter}}\right) * (2 * rand(0, 1) - 1) \right| \tag{57}$$

where t refers to the iteration number, while Max_{iter} represents the maximum number of iterations.

4) INITIALIZATION OF JELLYFISH POPULATION

In normal, Jellyfish population is randomly initialized. This population approach has some disadvantages such as trapping at local optimal solution and the slow convergence. There are many chaotic maps have been advanced to enhance the initial population diversity including tent map, Liebovitch map, and logistic map. In this study, the logistic map is used because it helps in providing more diversity in initial populations than the diversity of random initialization. It also reduces the premature convergence probability.

$$X_{i+1} = \eta_s X_i(1 - X_i), \quad 0 \leq X_o \leq 1 \tag{58}$$

where, X_i refers to the logistic chaotic value of i^{th} jellyfish location, η is a parameter set to 4.0, and X_o is used to generate the initial population of jellyfish, where $X_o \in (0, 1)$, $X_o \notin \{0.0, 0.25, 0.75, 0.5, 1.0\}$.

5) BOUNDARY CONDITIONS

Depending on the fact of spherically of the earth and oceans are found around it, when a jellyfish leaves the bounded of search area, it will automatically go back to the opposite bound of the area. This re-entering procedure

TABLE 4. JS algorithm.

JS inputs	• Define the objective function f(X) • Number of variables, nd (nd = 11 in this study) • Number of population, N_{Pop} (N_{Pop} = 100 considered) • Maximum Number of Iterations, MaxIt=1000 • Minimum and maximum values of nd -decision variables, in vector form Var_{min} and Var_{Max}
Initialization	• Initialize population of jellyfish X_i (i=1,2,….., N_{Pop}) using logistic chaotic map • Initialize time, t=1
Evaluate population	• Calculate the objective function at each X_i, f(X_i) • Find the best values of decision variables and the corresponding best value of the objective function
JS main loop	• Calculate time control C(t) using (57) • Set C_o =0.5 • If its value exceeded C_o, the jellyfish follow the ocean current using (51) • Check bound conditions using Eq.56 and calculate the objective function at the new location • Update the location of jellyfish (X_i) and location of jellyfish currently with the best objective function • If its value is less than C_o, they move inside the swarm ▪ If rand (0, 1) exceeded (1 −C (t)), the jellyfish exhibits type A motion and the new location of jellyfish is defined by (52) ▪ If rand (0, 1) is lower than (1 −C (t)), the jellyfish exhibits type B motion using (55) and the new location of jellyfish is defined by (56) • Check bound conditions using (59) and calculate the objective function at the new location • Update the location of jellyfish (X_i) and location of jellyfish currently with the best objective function • Continue the loop until reach N_{Pop}
Stopping criteria	• Update the time: t= t+1 until stopping criteria is met (t> MaxIt)

is presented by (59).

$$\begin{cases} X'_{i,d} = (X_{i,d} - U_{b,d}) + L_b(d) & if\ X_{i,d} > U_{b,d} \\ X'_{i,d} = (X_{i,d} - L_{b,d}) + U_b(d) & if\ X_{i,d} < L_{b,d} \end{cases} \quad (59)$$

where $X_{i,d}$ represents the i^{th} jellyfish location in a dimension (d^{th}), $X'_{i,d}$ refers to the updated location of the i^{th} jellyfish after checking the boundary constraints. While $L_{b,d}$ and $U_{b,d}$ are lower and upper bounds of the d^{th} dimension in food search spaces, respectively.

6) SCHEMATIC REPRESENTATION OF JS ALGORITHM

Exploration and exploitation phases represent the two key phases of a metaheuristic optimization algorithm. In the JS optimization algorithm, the motion of jellyfish in the direction of an ocean current represents the exploration phase and the motion inside a jellyfish swarm represents the exploitation phase, and the switching process between them is implemented using a time control mechanism. In the beginning, the exploration probability is higher than the exploitation probability because in this time jellyfish try to discover areas that includes promising optimal locations; as time passes on, the exploitation probability exceeds the exploration probability, and hence the jellyfish recognize the best position inside the discovered areas. Table 4 and Fig.5 illustrate the algorithm and flowchart of the JS optimization algorithm, respectively.

V. CASE STUDIES AND SIMULATION RESULTS

In this section, different case studies are executed for the modified IEEE-30 bus system. Results of the various case studies using the proposed Jellyfish search (JS) optimization algorithm are presented and explained. To verify the validity of JS optimization algorithm, four different optimization algorithms: ABC, CGO, FPA, and GPC are applied.

The results obtained by JS optimization algorithm are compared with the results obtained by the four above mentioned optimization algorithms and the results obtained by SHADE-SF in [42].

Case studies one and two are applied to study the impact of change of schedule wind and solar powers and PDF parameters on the generation costs. In the remaining case studies, the aim is to optimize the schedule generation from all sources under theoretical and practical conditions.

MATLAB software is used to perform the simulation of optimization techniques with computer properties: Intel (R) Core (TM) i3 CPU M380 @2.53 GHz and installed memory (RAM) 4 GB.

After running the algorithm five times, the optimal value of the objective function of each case study is found and control variables settings are listed, a maximum of 1000 iterations are implemented as the ending condition.

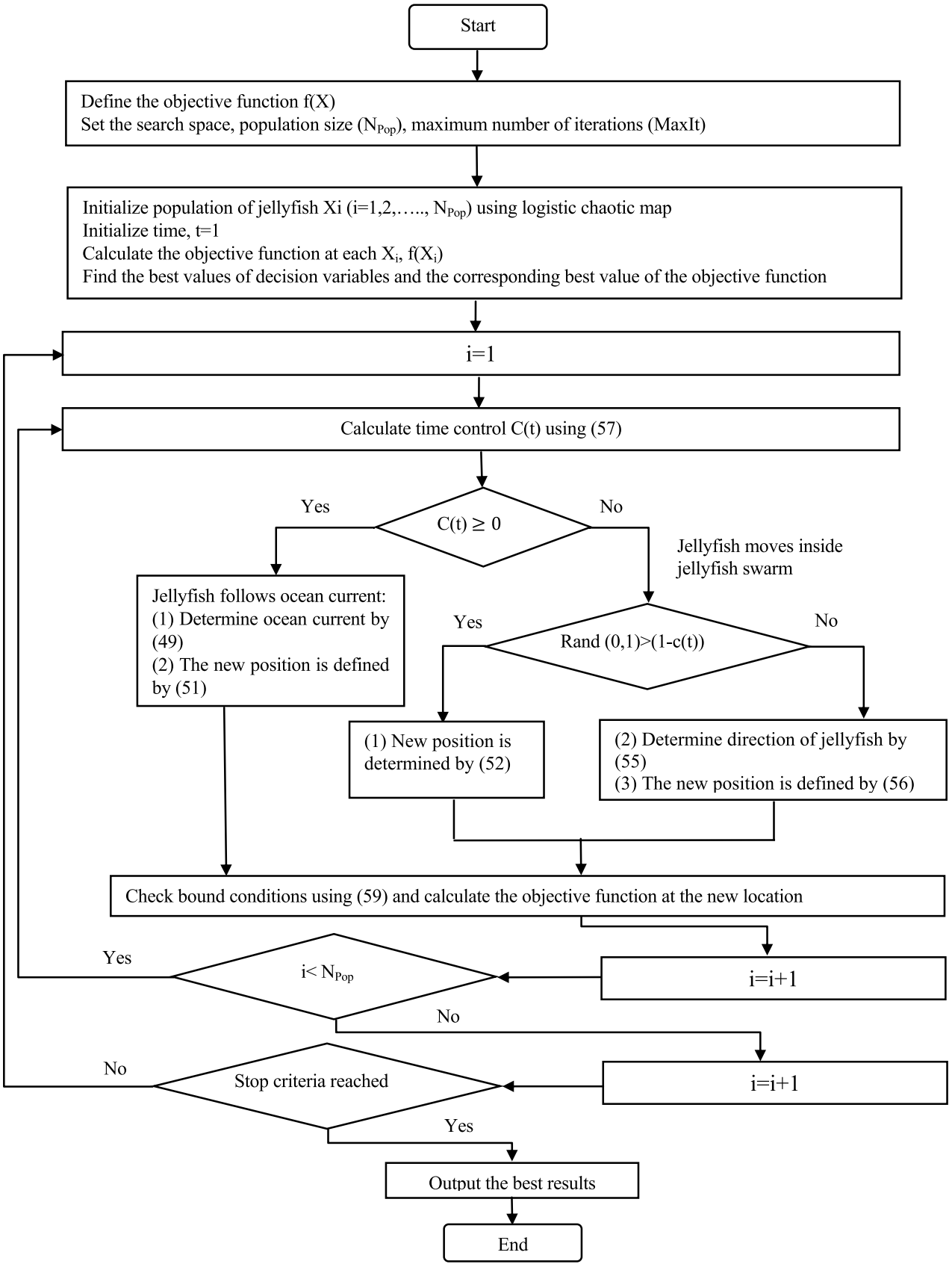

FIGURE 5. Schematic flowchart of JS algorithm.

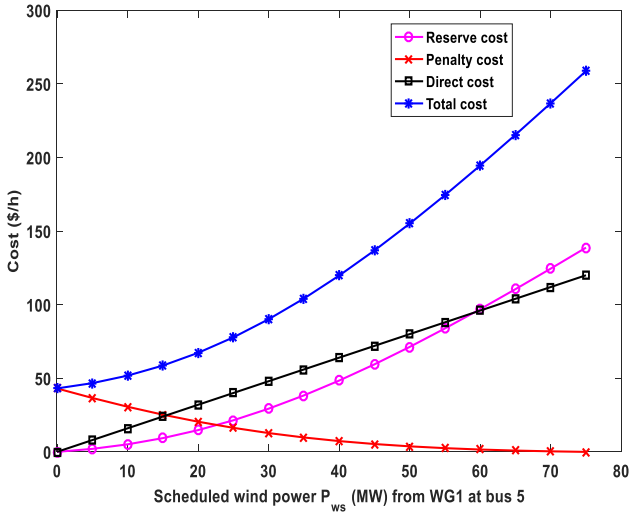

FIGURE 6. Variation of different wind power costs vs. scheduled power of wind power generator 1.

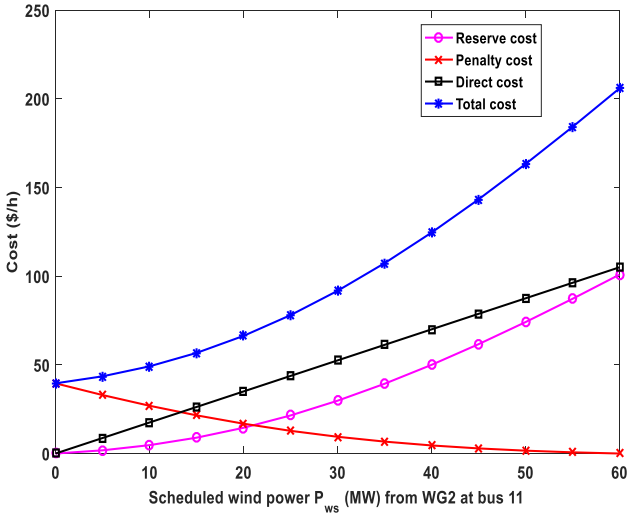

FIGURE 7. Variation of different wind power costs vs. scheduled power for wind power generator 2.

A. CASE-1: SCHEDULED OUTPUT POWER OF WIND AND SOLAR POWER PLANTS AGAINST DIFFERENT COSTS

In this case, the parameters of Weibull PDF are the same as provided in Table 3. Relevant parameters of wind turbine are presented in section III.A. The coefficients of direct cost for the wind power are g_1 =1.6 and g_2 = 1.75. The coefficients of penalty cost for not fully using wind power are $K_{PW,1} = K_{PW,2} = 1.5$ and the coefficients of reserve cost corresponding to overestimation of wind power are assumed $K_{RW,1} = K_{RW,2} = 3$. Noteworthy, the direct cost of wind and solar powers is lower than the average cost value of thermal power and the penalty cost for not utilizing wind power is lower than the direct cost [59]. For wind farm, the scheduled power varies from 0 to rated power and Figs. 6 and 7 show variations of total, direct, reserve, and penalty costs for the two wind farms. The total cost refers to the summation of direct, penalty and reserve costs in proportional to the scheduled wind power.

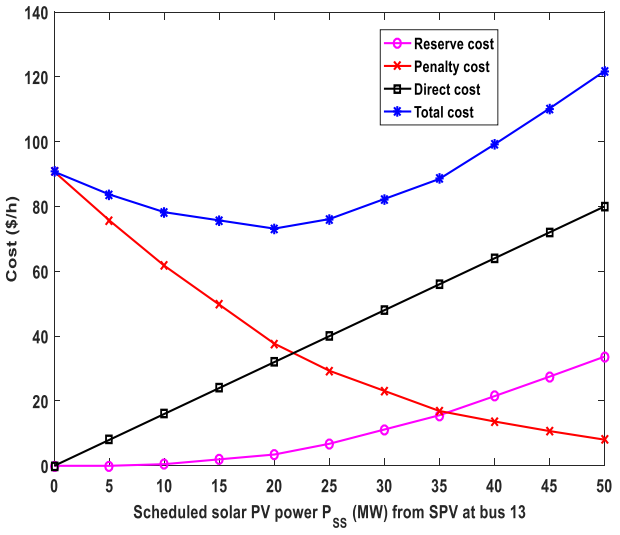

FIGURE 8. Variation of different solar power costs vs. schedule power for solar PV power generator.

In a similar way, Fig. 8 shows variations of total, direct, reserve, and penalty costs for solar PV power plant corresponding to the schedule solar power.

Based on Ref. [60], the yearly cost needed for operating and maintenance of a solar PV power plant lies almost in a range similar to that of the onshore type of wind power plants. Thus, in this work, the direct, reserve and penalty cost coefficients related to the solar PV power plant are assumed to be h = 1.6, K_{RS} = 3 and K_{PS} = 1.5 respectively. Any other parameters related to the solar PV power plant are provided in section III.A. It is worth to be mentioned, the total cost for solar power does not increase uniformly with increasing of the scheduled power of the solar PV power plant with the selected lognormal PDF parameters. Actually, the minimum total cost of solar PV power plant is achieved at around 20 MW of the scheduled power.

B. CASE 2: PROBABILITY DENSITY FUNCTION PARAMETER OF WIND AND SOLAR POWER PLANTS AGAINST DIFFERENT COSTS

This case is presented to study the change in wind power costs for a fixed arbitrarily schedule power with the variation of Weibull distribution scale parameter (c) (with fixed shape parameter for the two wind farms, k = 2). The schedule powers for WG1 and WG2 are fixed at one third of their installed capacity, i.e. 25MW and 20 MW, respectively. This assumption is reasonable since a practical wind power plant's capacity factor lies in a range from 30% to 45% [37]. Cost coefficients for the two wind farms are the same as used in case 1. Figs. 9 and 10 show variations of costs with the variation of the Weibull scale parameter for wind power plant 1 and wind power plant 2 respectively.

The minimum total cost for wind power is achieved at the middle value of the selected range for the scale parameter. With the increase of the scale parameter value, there will

TABLE 5. Simulation results of case-3 for the modified IEEE-30 bus system.

Control variables	Min	Max	JS	ABC	CGO	FPA	GPC	SHADE-SF [42]
P_{TG1} (MW)	50	140	134.9052	134.9309	134.907983	134.9094	134.9282	134.908
P_{TG2} (MW)	20	80	29.02269	26.94372	29.00926022	28.22249	29.32208	28.564
P_{TG3} (MW)	10	35	10.00067	10.01497	10.00003698	10.00032	10	10
$P_{Ws,1}$ (MW)	0	75	43.96969	43.18642	44.03747261	42.34021	43.39761	43.774
$P_{Ws,2}$ (MW)	0	60	37.01936	35.7538	37.17367089	36.51209	37.61635	36.949
P_{Ss} (MW)	0	50	34.25321	38.37797	34.04009624	37.27919	33.97897	34.976
V_1 (p.u.)	0.95	1.1	1.072501	1.071527	1.071751843	1.06979	1.068736	1.072
V_2 (p.u.)	0.95	1.1	1.056958	1.056271	1.056901004	1.056276	1.050177	1.057
V_5 (p.u.)	0.95	1.1	1.035078	1.034615	1.034863965	1.027006	1.036031	1.035
V_8 (p.u.)	0.95	1.1	1.070583	1.039293	1.098399047	1.07472	1.09672	1.04
V_{11} (p.u.)	0.95	1.1	1.0983	1.095292	1.098294991	1.088097	1.098845	1.1
V_{13} (p.u.)	0.95	1.1	1.045714	1.047535	1.048718843	1.061001	1.1	1.055
Parameters								
Q_{TG1} (MVAr)	-20	150	-0.68357	-1.22952	-2.453131685	-5.54808	2.768697	-1.903
Q_{TG2} (MVAr)	-20	60	11.01158	13.00946	12.08045192	19.59481	-6.70158	13.261
Q_{TG3} (MVAr)	-15	40	40	36.64525	40	40	40	35.101
$Q_{Ws,1}$ (MVAr)	-30	35	22.66739	23.79469	22.33924071	16.20713	27.39157	23.181
$Q_{Ws,2}$ (MVAr)	-25	30	30	29.63638	30	26.42068	28.96604	30
Q_{Ss} (MVAr)	-20	25	14.02464	15.24326	15.03625504	20.48	25	17.346
Total cost ($/h)			**781.6387**	782.1535	782.1950203	782.8596	782.4229	782.503
Emission (t/h)			1.761998	1.764966	1.761969598	1.762312	1.764097	1.762
Carbon tax ($/h)			0	0	0	0	0	0
P_{loss} (MW)			5.773893	5.807766	5.768519947	5.863689	5.843226	5.77
V_d (p.u.)			0.448284	0.442165	0.45382503	0.455137	0.537061	0.463

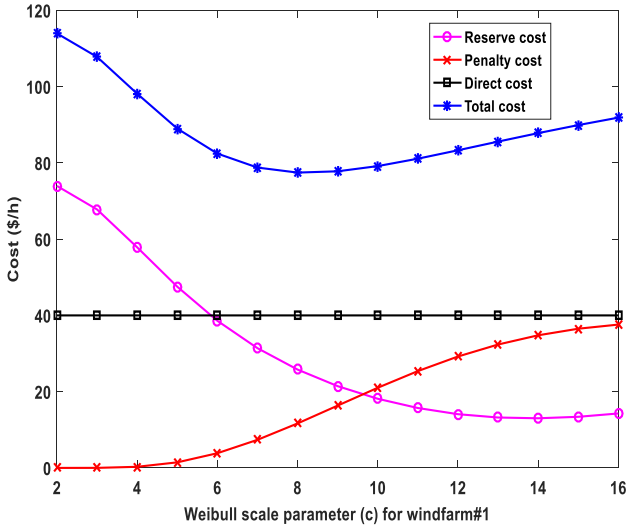

FIGURE 9. Variation of different wind power costs vs. Weibull scale parameter (c) for wind power generator 1 (bus 5).

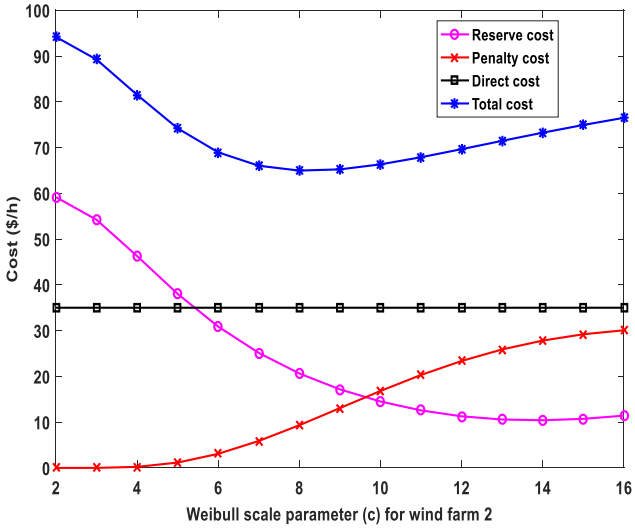

FIGURE 10. Variation of wind power cost vs Weibull scale parameter (c) for wind farm 2 (bus 11).

be a domination of wind speeds with specific probabilities. With keeping the scheduled power the same, the penalty cost increases leading to raise the total cost. However, the level of reduction in the reserve cost is insignificant above a certain value of the Weibull scale parameter.

For evaluating the variation in the cost of solar PV power with the change in the mean of the lognormal PDF (μ), the value of μ is changed with an increase value of 0.5 in a range from 2 to 7. The scheduled power of solar PV plant is constant at 20 MW with standard deviation (σ) = 0.6. Cost coefficients for the solar PV plant are the same as used in case 1. Fig. 11 illustrates cost curves for solar power. From Fig.11, it is clear that the total cost of solar power is gradually reducing to its minimum value at lognormal mean

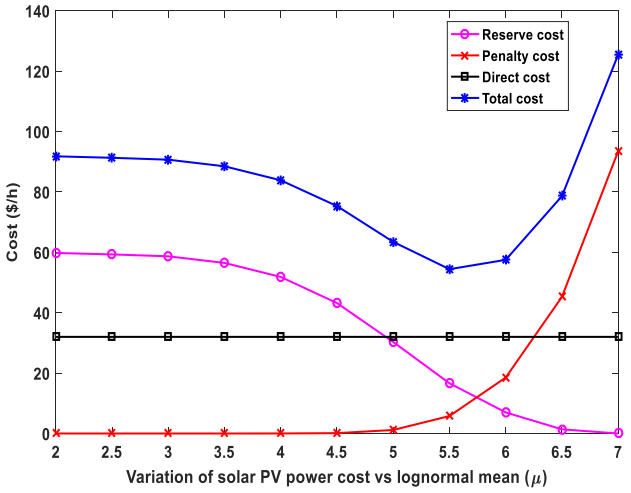

FIGURE 11. Variation of different solar PV power costs vs. lognormal mean (μ) for SPV (bus 13).

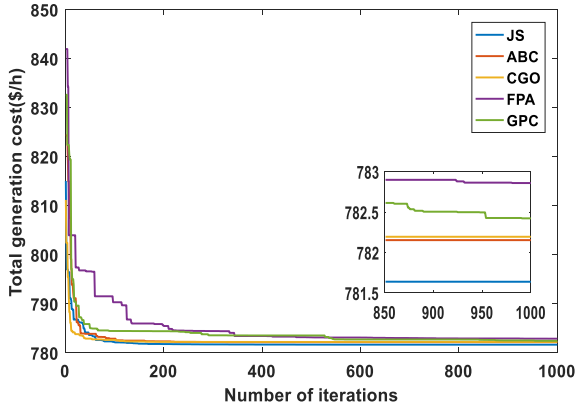

FIGURE 12. Convergence characteristics of different optimization techniques for case-3.

(μ) = 5.5. It is also clear that the reserve cost and penalty cost are the same at about lognormal mean = 5.8. After this value, the penalty cost increase sharply, leading to suddenly increasing in the total cost of solar PV power.

It is necessary to select an appropriate value of the scheduled power of solar PV due to the high sensitivity of solar irradiance for the value of μ and consequently the solar power. When the value of μ is low, solar irradiance is low and consequently the output power is also low, thus approximately the full reserve power is necessary to compensate the output power.

However, if the value of μ is high, the solar irradiance will be high and consequently the solar PV output power will be high.

C. CASE-3: TOTAL GENERATION COST MINIMIZATION

Case-3 is implemented for optimization the scheduled power of both conventional and renewable power generators to minimize the total generation cost depending on Eq.11.

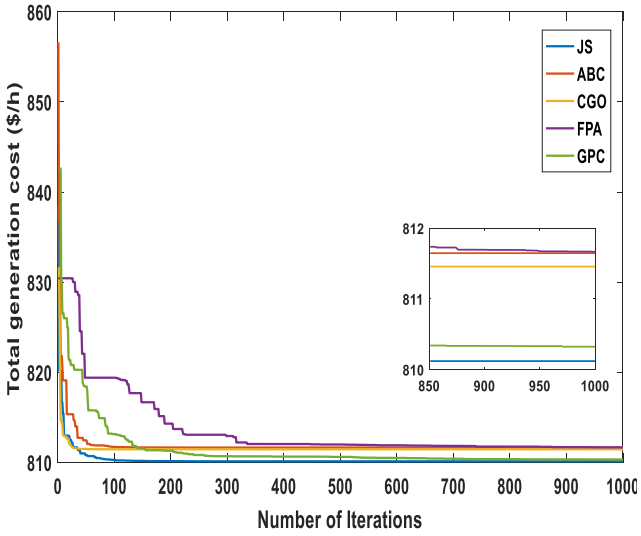

FIGURE 13. Convergence characteristics of different optimization techniques for case-4.

A comparison between the convergences of different OPF optimization methods is provided by Fig. 12. Table 5 provides the optimal results of total generation cost, reactive power (Q), control variables, and other important calculated parameters. For clarification, V_i refers to the i-th bus voltage, $P_{Ws,1}$ and $P_{Ws,2}$ represent the scheduled output power from wind farm 1 and wind farm 2, respectively, and P_{Ss} represents the solar PV schedule power. P_{loss} and V_d refer to power loss and voltage deviation that are calculated by Eqs. 24-25, respectively. Simulation results of case 3 show the effectiveness of JS algorithm, fast convergence, and high solution quality comparing to the other OPF optimization algorithms. The minimum total generation cost reached by JS is **781.64**. Consequently, for this case, JS exceeds SHADE-SF [42] in addition to all other applied optimization algorithms regarding minimization of total generation cost and solution convergence.

D. CASE-4: MINIMIZATION OF TOTAL GENERATION COST WITH CARBON EMISSION TAX

This case study aims at minimizing the total cost of generation considering the carbon tax (Ct) imposed on the conventional power sources due to their emissions of CO_2 based on Eq. 12. For this case, the imposed carbon tax is assumed to be \$20/ton [42]. It is expected with the existence of the carbon tax, increasing the level of penetration from renewable energy sources, and this concept is clear from simulation results. The level of penetration of solar PV and wind powers in the schedule of optimum generation is solely depending on the volume of carbon emissions and the value of imposed carbon tax. For this case, Fig. 13 provides a comparison between the convergence of JS optimization technique and other applied techniques.

For this case study, Table 6 provides the optimal results of total generation cost, reactive power (Q), control variables, and other important calculated parameters.

TABLE 6. Simulation results of case-4 for the modified IEEE-30 bus system.

Control variables	Min	Max	JS	ABC	CGO	FPA	GPC	SHADE SF [42]
P_{TG1} (MW)	50	140	123.5721	123.4582184	123.7418	124.1334	124.0029	123.525
P_{TG2} (MW)	20	80	33.1626	33.06898382	33.6837	34.22647	34.00827	33.047
P_{TG3} (MW)	10	35	10	10	10	10.01113	10	10
$P_{Ws,1}$ (MW)	0	75	46.0806	45.98766679	46.35961	46.6678	46.39491	46.021
$P_{Ws,2}$ (MW)	0	60	38.8011	38.78372149	39.0181	38.57113	39.04157	38.748
P_{Ss} (MW)	0	50	37.0628	37.37551975	35.97478	35.0977	35.27946	37.336
V_1 (p.u.)	0.95	1.1	1.07066	1.070444664	1.07163	1.070194	1.06967	1.071
V_2 (p.u.)	0.95	1.1	1.05715	1.057030608	0.952155	1.055241	1.054404	1.057
V_5 (p.u.)	0.95	1.1	1.03604	1.035968679	1.089148	1.038628	1.030943	1.036
V_8 (p.u.)	0.95	1.1	1.04038	1.040631609	1.04196	1.052149	1.099904	1.04
V_{11} (p.u.)	0.95	1.1	1.0983	1.098363277	1.099785	1.095573	1.086781	1.099
V_{13} (p.u.)	0.95	1.1	1.05575	1.055751513	1.062462	1.053955	1.099938	1.056
Parameters	Min	Max	JS	ABC	CGO	FPA	GPC	SHADE-SF [42]
Q_{TG1} (MVAr)	-20	150	-2.66665	-2.931556238	13.20645	-0.37942	-0.13942	-2.678
Q_{TG2} (MVAr)	-20	60	12.35409	12.27265344	-20	4.145923	6.648286	12.319
Q_{TG3} (MVAr)	-15	40	35.25438	35.68511796	37.7156	40	40	35.27
$Q_{Ws,1}$ (MVAr)	-30	35	22.99902	22.93901908	35	25.94203	19.02155	22.964
$Q_{Ws,2}$ (MVAr)	-25	30	30	30	30	28.84476	25.05216	30
Q_{Ss} (MVAr)	-20	25	17.71142	17.68837052	20.10166	17.01849	25	17.779
Total cost ($/h)			**810.1201**	811.6468942	811.4568	811.6664	810.324	810.346
Emission (t/h)			0.89377	0.887943299	0.902467	0.923031	0.916127	0.891
Carbon tax ($/h)			17.8754	17.75886598	18.04935	18.46063	18.32254	17.82
P_{loss} (MW)			5.276	5.274110229	5.377988	5.307636	5.327113	5.276
V_d (p.u.)			0.46884	0.46931046	0.499635	0.465664	0.507454	0.469

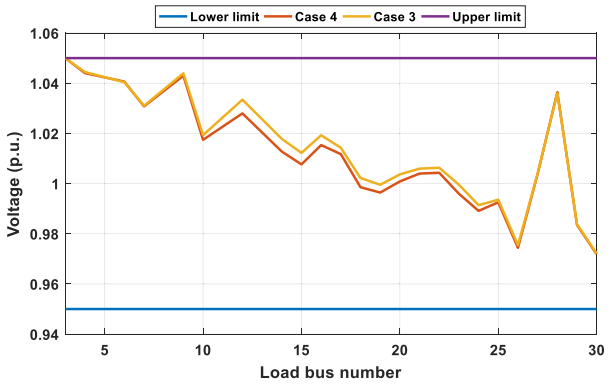

FIGURE 14. Load bus voltage profiles for case-3 and case-4.

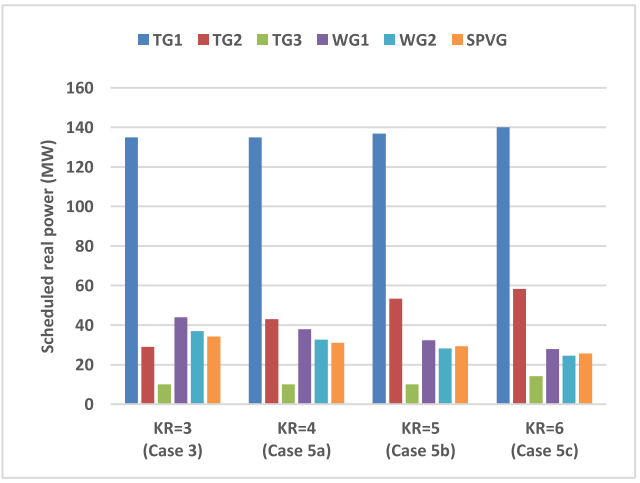

FIGURE 15. Variation of optimal scheduled real power (MW) with variation of reserve cost coefficient (KR).

The minimum generation cost achieved by JS is **810.1201**. It is also clear that, for this case, JS exceeds SHADE-SF [42] in addition to all other applied algorithms regarding minimization of total cost and solution convergence.

The voltages of load buses (PQ buses) represent very important factor in OPF. Thus, it is necessary to critically addressee the constraints related to voltages of load buses. In IEEE- 30 bus system, operating voltages of all load buses must be inside the range from 0.95 to 1.05 p.u.

In this aspect, Fig. 14 presents voltage profiles of PQ buses for Case-3 in addition to Case-4. Fig.14 shows that all PQ buses voltages are within limits after optimization for the two case studies.

E. CASE-5: OPTIMIZED COST AGAINST RESERVE COST

In this case, all parameters are keeping as in Case 3 excluding coefficients of reserve cost. Coefficients of reserve cost for both solar PV and wind powers are changed from $K_{RS} = K_{RW,1} = K_{RW,2} = K_R = 4$ to $K_R = 6$ with incremental step of one. The coefficient of penalty cost for both solar PV and wind powers is $K_{PS} = K_{PW,1} = K_{PW,2} = K_P = 1.5$ as used in both Case 1 and Case 3. Fig. 15 indicates the optimized schedule power of all generators in a bar chart form. For clarification, Case 5a represents the case when

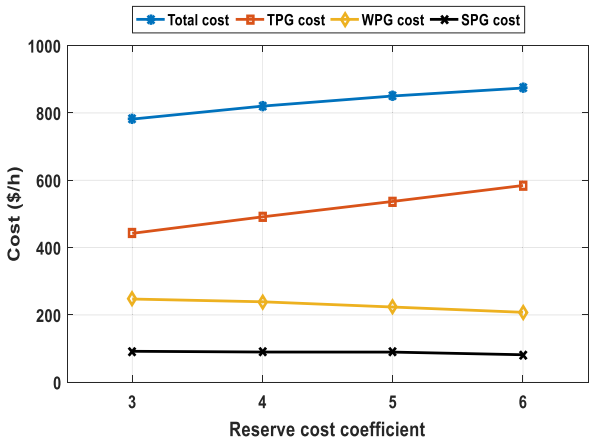

FIGURE 16. Curves of costs with change in reserve cost (KR) coefficient.

$K_R = 4$, Case 5b represents $K_R = 5$, and Case 5c represents $K_R = 6$. When the coefficient of reserve cost increases, the optimal scheduled power from wind and solar PV plants reduces as decreasing the scheduled output power needs a lesser amount of spinning reserve. Thermal power generators compensate the shortage of output power from wind and solar PV sources. Hence, the cost of thermal power generator increases as noted from the profile of thermal power generator cost (TPG) in Fig. 16. Costs of solar PV generator (SPG) and wind power generator (WPG) gradually reduces to an amount. WPG cost comprises cost of output power from the two wind generators. Total power cost increases with the increase in the coefficient of reserve cost.

F. CASE-6: OPTIMIZED COST AGAINST PENALTY COST

In this case, all parameters are keeping as in Case 3 excluding coefficients of penalty cost. Coefficients of the penalty cost for both solar and wind power are increased from $K_{PS} = K_{PW,1} = K_{PW,2} = K_P = 1.5$ to $K_P = 3$ for Case 6a, $K_P = 4$ for Case 6b and $K_P = 5$ for Case 6c. The coefficient of reserve cost for both solar PV and wind powers is $K_{RS} = K_{RW,1} = K_{RW,2} = K_R = 3$ as used in both Case 1 and Case 3. Similar to Case 5, Fig. 17 presents the optimized schedule power of all generators in a bar chart form. When the coefficient of penalty cost increases, the optimal scheduled power from wind and solar PV plants increases as increasing the scheduled output power helps in reducing the penalty cost when solar irradiance or wind speed is high. However, the manner, in this case, is different from Case 5 as the increase of scheduled power seems not to uniform for all renewable energy sources. This different can be interpreted by the extremely non-linear relations between the probability distribution functions and reserve or penalty cost of both solar PV and wind power. Fig. 18. shows a progressive increase in wind power generator cost (WPG cost) with a small fluctuation in the cost of solar PV power (SPG cost) due to the fluctuating of its scheduled output power. It is also noted that the cost of thermal power generation (TPG cost) is nearly constant and a steady rise in total cost is observed.

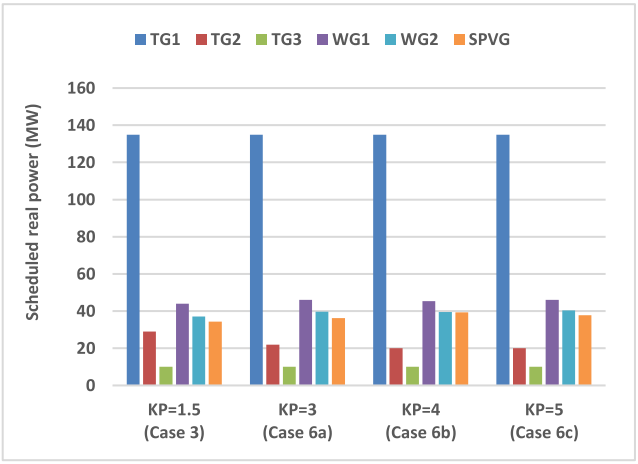

FIGURE 17. Variation of optimal scheduled real power (MW) with change in penalty cost coefficient.

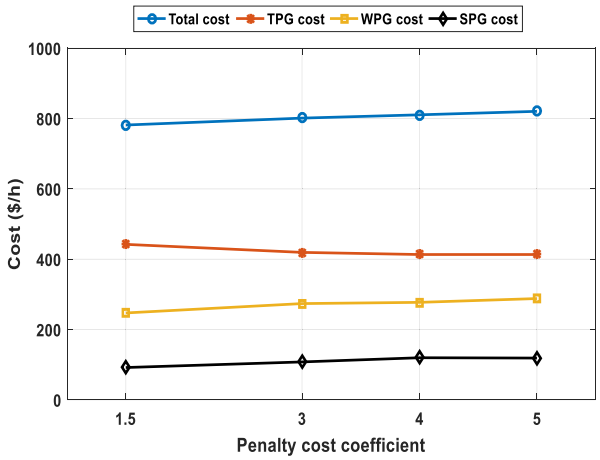

FIGURE 18. Curves of costs with change in penalty cost (KP) coefficient.

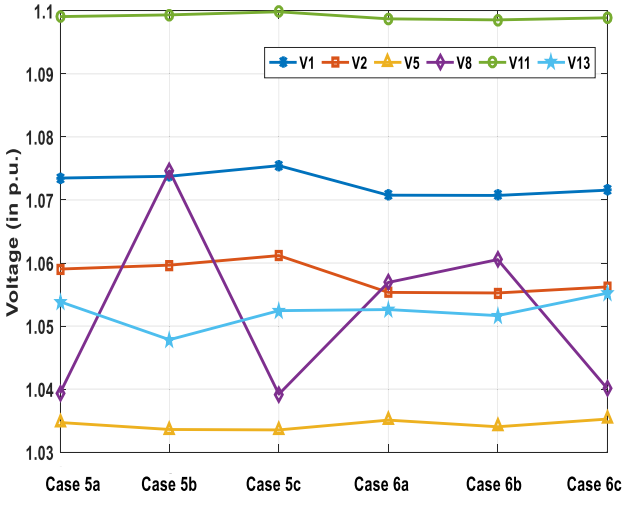

FIGURE 19. Voltage profiles of PV buses for case 5 and case 6.

Fig. 19 presents the voltage of all generator buses in the modified IEEE- 30 bus system for all the situations of varying penalty and reserve costs implemented under

TABLE 7. Simulation results of case-7 (considering ramp rate effect) for the modified IEEE-30 bus system.

Control variables	Min	Max	JS	ABC	CGO	FPA	GPC	SHADE SF
P_{TG1} (MW)	79.211	114.211	93.0823	96.72472	98.6741	93.56576	91.48802	95.60649
P_{TG2} (MW)	65	80	65	65.00008	65	65	65	65
P_{TG3} (MW)	12	24	12	12	12	12	12	12
$P_{Ws,1}$ (MW)	0	75	44.10123	43.69526	43.44613	44.64553	44.67372	43.86249
$P_{Ws,2}$ (MW)	0	60	37.277	37.01419	36.76069	38.08724	37.17865	37.09953
P_{Ss} (MW)	0	50	36.59075	33.75484	32.38663	34.76074	37.69296	34.58041
V_1 (p.u.)	0.95	1.1	1.067719	1.068438	1.068877	1.066272	1.069933	1.067618
V_2 (p.u.)	0.95	1.1	1.058899	1.059353	1.05947	1.056407	1.060794	1.058544
V_5 (p.u.)	0.95	1.1	1.037209	1.036794	1.037329	1.038319	1.033251	1.036748
V_8 (p.u.)	0.95	1.1	1.04168	1.041847	1.041501	1.050983	1.033528	1.099966
V_{11} (p.u.)	0.95	1.1	1.099714	1.099915	1.1	1.095926	1.099389	1.099728
V_{13} (p.u.)	0.95	1.1	1.057501	1.055549	1.056079	1.051801	1.099902	1.051754
Parameters	Min	Max	JS	ABC	CGO	FPA	GPC	SHADE-SF
Q_{TG1} (MVAr)	-20	150	-4.59964	-4.61954	-4.27311	-2.97062	-1.9863	-4.87838
Q_{TG2} (MVAr)	-20	60	11.3628	12.28351	11.8896	5.412819	18.54202	10.20858
Q_{TG3} (MVAr)	-15	40	35.39301	36.08666	35.48585	40	22.13671	40
$Q_{Ws,1}$ (MVAr)	-30	35	23.33904	22.82225	23.46733	25.74383	19.92593	22.68444
$Q_{Ws,2}$ (MVAr)	-25	30	30	30	30	29.07318	30	30
Q_{Ss} (MVAr)	-20	25	17.99892	17.29605	17.51477	16.33654	25	15.74273
Total cost ($/h)			**804.1093**	804.8701	805.2522	804.6703	804.906	804.4638
Emission (t/h)			0.210904	0.240613	0.259541	0.214468	0.199885	0.23076
Carbon tax ($/h)			0	0	0	0	0	0
P_{loss} (MW)			4.651976	4.789091	4.86755	4.659303	4.633354	4.748927
V_d (p.u.)			0.48309	0.475469	0.477006	0.458484	0.520446	0.469148

TABLE 8. Loading scenarios and their probabilities [63].

Loading scenarios	% Loading, P_d (Mean)	Scenario probability, Δ_{sc}
Scenario 1	54.749	0.15866
Scenario 2	65.401	0.34134
Scenario 3	74.599	0.34134
Scenario 4	85.251	0.15866

Case 5 and Case 6. The voltages of all generator buses are inside the stated range (0.95 - 1.10 p.u.).

Fig. 20 illustrates the schedule reactive power from all generators. By observing the limits of reactive power (Q) provided in Table 5, generators TG3 and WG2 operate at their maximum limits of Q capability for several cases. So, it is necessary to consider the constraints on Q during implementation of any optimization algorithm.

G. CASE-7: MINIMIZATION OF TOTAL GENERATION COST WITH RAMP RATE LIMITS OF THERMAL GENERATORS

Case-7 is implemented to optimize the scheduled power of both conventional and renewable power generators to minimize the total generation cost depending on (11) in more practical conditions through considering the effect of ramp rate limits of thermal power generators.

The power generation at the previous hour for the thermal power generators and their down and up ramp-rate limits are presented in Table 2 [61].

For this case, the optimal results of total generation cost, reactive power (Q), control variables, and other important calculated parameters are recorded in Table 7.

A comparison between the convergence characteristics of different OPF optimization methods used in this case study is provided by Fig. 21.

Comparing the results between Table 5 (Case 3) and Table 7 (Case 7), the increase in the total generation cost is clear as expected due to considering the ramp rate limits of thermal generators. The results prove also the effectiveness of the JS algorithm, fast convergence, and high solution quality compared with the other OPF optimization algorithms. The minimum total generation cost reached by JS is 804.10927. Consequently, for this practical case, JS exceeds SHADE-SF in addition to all other applied optimization algorithms regarding minimization of total generation cost and solution convergence.

Table 7 demonstrates that all algorithms duly satisfy all system constraints.

Fig.22 shows the PQ buses voltage profile for Case-7. From this figure, it can be observed that all PQ buses voltages are within limits for this case study.

H. CASE-8: CASE STUDY CONSIDERING UNCERTAINTIES IN LOAD DEMAND

In this case, a realistic condition of variable load demand is presented. A normal probability density function (PDF)

TABLE 9. Simulation results of case-8 (loading scenario 1).

Control variables	Min	Max	JS	ABC	CGO	FPA	GPC	SHADE SF
P_{TG1} (MW)	50	140	50	50.01717	50.00001	50.01919	50.01788	50
P_{TG2} (MW)	20	80	20	20	20.00008	20.01538	20.00455	20
P_{TG3} (MW)	10	35	10	10	10.00001	10.0121	10	10
$P_{Ws,1}$ (MW)	0	75	27.11415	28.11119	25.98063	27.4725	26.20593	27.16875
$P_{Ws,2}$ (MW)	0	60	23.86485	23.62546	22.47809	24.36508	26.55242	23.5009
P_{Ss} (MW)	0	50	25.33448	24.57271	28.22598	24.49292	23.75082	25.64634
V_1 (p.u.)	0.95	1.1	1.056831	1.049757	1.051226	1.043419	1.054116	1.056862
V_2 (p.u.)	0.95	1.1	1.051193	1.041122	1.098626	1.018121	0.977155	1.051217
V_5 (p.u.)	0.95	1.1	1.040 821	1.030449	1.029804	1.026693	1.02382	1.040829
V_8 (p.u.)	0.95	1.1	1.044518	1.035291	1.03566	1.032241	1.065382	1.044461
V_{11} (p.u.)	0.95	1.1	1.081709	1.074026	1.035221	1.057582	1.055512	1.081605
V_{13} (p.u.)	0.95	1.1	1.048499	1.051181	1.018581	1.049319	1.066503	1.048479
Parameters	Min	Max	JS	ABC	CGO	FPA	GPC	SHADE-SF
Q_{TG1} (MVAr)	-20	150	-5.67008	0.368158	-20	4.964277768	3.555286	-5.63767
Q_{TG2} (MVAr)	-20	60	-1.36206	-8.33559	60	-20	-20	-1.31239
Q_{TG3} (MVAr)	-15	40	13.33735	12.25639	4.808939	18.14271464	40	13.28396
$Q_{Ws,1}$ (MVAr)	-30	35	8.996774	7.88354	-8.41553	11.63164	-4.83782	8.992761
$Q_{Ws,2}$ (MVAr)	-25	30	17.38505	17.09758	5.054589	13.15988147	7.239673	17.35138
Q_{Ss} (MVAr)	-20	25	6.80286	10.85521	-0.6754	12.72406676	14.32227	6.794837
Total cost ($/h)			**409.6387**	410.0328	411.2637	410.6641	410.9653	409.7087
Emission (t/h)			0.104028	0.104036	0.104028	0.104029	0.104035	0.104028
Carbon tax ($/h)			0	0	0	0	0	0
P_{loss} (MW)			1.155807	1.16887	1.577414	1.219467	1.373935	1.158328
V_d (p.u.)			0.734327	0.58037	0.377185	0.448335	0.782838	0.733124

TABLE 10. Simulation results of case-8 (loading scenario 2).

Control variables	Min	Max	JS	ABC	CGO	FPA	GPC	SHADE SF
P_{TG1} (MW)	50	140	53.07501	51.58378	51.15181	52.5423	50.53026	50
P_{TG2} (MW)	20	80	21.1214	20.85461	20.76967273	21.52551	20.4415	20.49794
P_{TG3} (MW)	10	35	10	10	10	10.00572	10	10
$P_{Ws,1}$ (MW)	0	75	38.1028	37.96523	37.9004	38.53796	37.46345	37.72788
$P_{Ws,2}$ (MW)	0	60	32.7427	32.58934	32.54333	32.89925	32.15986	32.42119
P_{Ss} (MW)	0	50	31.72042	33.75501	34.59078	31.23999	36.22626	36.09066
V_1 (p.u.)	0.95	1.1	1.057585	1.057247	1.056902	1.057773	1.059201	1.056858
V_2 (p.u.)	0.95	1.1	1.051576	1.051346	1.050547	1.052153	1.053206	1.051115
V_5 (p.u.)	0.95	1.1	1.041038	1.040884	1.03888	1.041015	1.050123	1.040673
V_8 (p.u.)	0.95	1.1	1.044328	1.04437	0.950365	1.043593	1.036505	1.044338
V_{11} (p.u.)	0.95	1.1	1.089667	1.08969	1.1	1.087138	1.088191	1.089753
V_{13} (p.u.)	0.95	1.1	1.050963	1.051524	1.0754667	1.041703	1.060386	1.052473
Parameters	Min	Max	JS	ABC	CGO	FPA	GPC	SHADE-SF
Q_{TG1} (MVAr)	-20	150	-5.4184	-5.40855	-1.36652	-5.3636	-3.65332	-5.49675
Q_{TG2} (MVAr)	-20	60	0.550422	0.39186	9.904012	3.196724	0.49967	0.38892
Q_{TG3} (MVAr)	-15	40	17.917	17.92055	-15	18.3457	2.555362	17.76763
$Q_{Ws,1}$ (MVAr)	-30	35	11.608	11.6135	16.0459	11.58992	21.86297	11.60696
$Q_{Ws,2}$ (MVAr)	-25	30	21.75612	21.76554	27.39675	21.59022	21.52835	21.78341
Q_{Ss} (MVAr)	-20	25	9.297525	9.495981	20.68186	6.367405	13.28303	9.850481
Total cost ($/h)			**496.0327**	496.251	496.2825	496.5544	497.1111	496.1383
Emission (t/h)			0.105272	0.104525	0.104329	0.104828	0.104129	0.103857
Carbon tax ($/h)			0	0	0	0	0	0
P_{loss} (MW)			1.414821	1.400464	1.608478	1.403229	1.473813	1.390155
V_d (p.u.)			0.660391	0.661417	0.648737	0.593311	0.665491	0.663697

is used to model the uncertainty in load demand of the system [62]. A scenario-based methodology is implemented to achieve the optimization process at some discrete scenarios (levels) of load demand.

Fig. 23 describes the uncertain load demand with the normal distribution diagram. The horizontal axis of Fig. 23 represents the percentage of the network loading. The values of the mean (σ_d) and standard deviation (σ_d) of the PDF are

TABLE 11. Simulation results of case-8 (loading scenario 3).

Control variables	Min	Max	JS	ABC	CGO	FPA	GPC	SHADE SF
P_{TG1} (MW)	50	140	102.2613	88.83016	94.24286	89.34298	101.9919	102.0087
P_{TG2} (MW)	20	80	20	20	20	20.00553	20	20
P_{TG3} (MW)	10	35	10	10	10	10.00557	10.00389	10
$P_{Ws,1}$ (MW)	0	75	30.54907	33.87272	32.48259	33.60923	31.21616	30.60243
$P_{Ws,2}$ (MW)	0	60	26.25115	29.08305	27.89939	29.03022	25.92982	26.29866
P_{Ss} (MW)	0	50	25.60671	32.38658	29.73962	32.22193	25.57995	25.74868
V_1 (p.u.)	0.95	1.1	1.0656	1.063052	1.064141	1.061282	1.067907	1.065562
V_2 (p.u.)	0.95	1.1	1.05394	1.052958	1.053322	1.049003	1.057	1.053899
V_5 (p.u.)	0.95	1.1	1.036795	1.03718	1.037075	1.034103	1.051389	1.036776
V_8 (p.u.)	0.95	1.1	1.040962	1.041815	1.041389	1.041575	1.040453	1.040967
V_{11} (p.u.)	0.95	1.1	1.09806	1.097166	1.097649	1.084209	1.089676	1.098037
V_{13} (p.u.)	0.95	1.1	1.049185	1.051714	1.050593	1.046698	1.021449	1.049314
Parameters	Min	Max	JS	ABC	CGO	FPA	GPC	SHADE-SF
Q_{TG1} (MVAr)	-20	150	-3.75542	-4.6216	-4.07208	-0.32437	-3.52486	-3.70578
Q_{TG2} (MVAr)	-20	60	4.975995	4.215691	4.293338	-1.93086	4.185627	4.88314
Q_{TG3} (MVAr)	-15	40	20.72831	21.12707	20.83125	26.9174	18.94888	20.72654
$Q_{Ws,1}$ (MVAr)	-30	35	15.01725	14.52896	14.83059	14.69734	28.3975	14.9998
$Q_{Ws,2}$ (MVAr)	-25	30	25.99339	25.66101	25.84801	22.03495	24.39524	25.9829
Q_{Ss} (MVAr)	-20	25	10.25461	11.0825	10.69668	10.66087	0.879007	10.30029
Total cost ($/h)			**576.1951**	577.4485	576.2578	577.0696	576.6372	577.2079
Emission (t/h)			0.303825	0.186495	0.222362	0.189397	0.300363	0.300578
Carbon tax ($/h)			0	0	0	0	0	0
P_{loss} (MW)			3.255727	2.760013	2.951953	2.802973	3.309198	3.24596
V_d (p.u.)			0.572525	0.585415	0.579784	0.500011	0.433808	0.573021

TABLE 12. Simulation results of case-8 (loading scenario 4).

Control variables	Min	Max	JS	ABC	CGO	FPA	GPC	SHADE SF
P_{TG1} (MW)	50	140	134.9079	134.9088	134.9079	134.0265	134.8902	134.9079
P_{TG2} (MW)	20	80	20.00001	20.00662	20.00001	20.00059	20.01361	20
P_{TG3} (MW)	10	35	10	10.00189	10	10.00099	10	10
$P_{Ws,1}$ (MW)	0	75	30.45387	31.15208	30.95905	28.52346	31.08668	30.52827
$P_{Ws,2}$ (MW)	0	60	25.71961	26.65671	26.51802	23.75976	26.50585	26.13722
P_{Ss} (MW)	0	50	25.66037	23.985	24.33131	30.52704	24.35634	25.16048
V_1 (p.u.)	0.95	1.1	1.071524	1.070969	1.071579	1.074125	1.068388	1.071496
V_2 (p.u.)	0.95	1.1	1.05613	1.055886	1.05622	1.057987	1.053634	1.056129
V_5 (p.u.)	0.95	1.1	1.034638	1.033464	1.034715	1.029142	1.09999	1.034665
V_8 (p.u.)	0.95	1.1	1.039138	1.039546	1.039146	1.03967	1.031095	1.039172
V_{11} (p.u.)	0.95	1.1	1.099996	1.099422	1.099993	1.1	1.1	1.1
V_{13} (p.u.)	0.95	1.1	1.048812	1.051508	1.049076	1.021057	1.096912	1.049054
Parameters	Min	Max	JS	ABC	CGO	FPA	GPC	SHADE-SF
Q_{TG1} (MVAr)	-20	150	-1.67883	-2.54093	-1.70304	1.904877	-4.17854	-1.7463
Q_{TG2} (MVAr)	-20	60	9.94829	10.6052	10.07456	15.96648	1.853478	9.952276
Q_{TG3} (MVAr)	-15	40	26.01946	26.88535	25.94546	30.5	9.404693	26.01744
$Q_{Ws,1}$ (MVAr)	-30	35	18.88195	17.49405	18.71583	13.43872	35	18.8662
$Q_{Ws,2}$ (MVAr)	-25	30	28.36793	28.0106	28.35645	30	27.38144	28.35801
Q_{Ss} (MVAr)	-20	25	12.27954	13.33517	12.4165	2.658251	25	12.38007
Total cost ($/h)			**652.8243**	653.586	653.334	653.7401	653.7166	652.9029
Emission (t/h)			1.764578	1.764678	1.764577	1.671564	1.762655	1.764579
Carbon tax ($/h)			0	0	0	0	0	0
P_{loss} (MW)			5.139611	5.109	5.114136	5.236186	5.25056	5.131738
V_d (p.u.)			0.492754	0.503983	0.494803	0.398062	0.616049	0.494368

70 and 10, respectively. Fig. 23 includes four-color areas that represent the four considered different scenarios (levels) of system loading (P_d) in this case. The probability of occurrence of a certain loading scenario and its mean are given as [62].

$$\Delta_{sc,i} = \int_{P_{d,i}^{low}}^{P_{d,i}^{high}} \frac{1}{\sigma_d \sqrt{2\pi}} exp\left[\frac{(P_d - \mu_d)^2}{2{\sigma_d}^2}\right] dP_d \quad (60)$$

where, $\Delta_{sc,i}$ represents the probability of i-th scenario of loading, while $P_{d,i}^{low}$ and $P_{d,i}^{high}$ represent the low and high limits of i-th loading scenario, respectively.

$$\mathrm{P}_{D,i} = \frac{1}{\Delta_{sc,i}} \int_{P_{d,i}^{low}}^{P_{d,i}^{high}} \left(\frac{1}{\sigma_d \sqrt{2\pi}} exp\left[\frac{(P_d - \mu_d)^2}{2{\sigma_d}^2}\right]\right) dP_d \quad (61)$$

where, $\mathrm{P}_{D,i}$ is the mean of i-th level of loading.

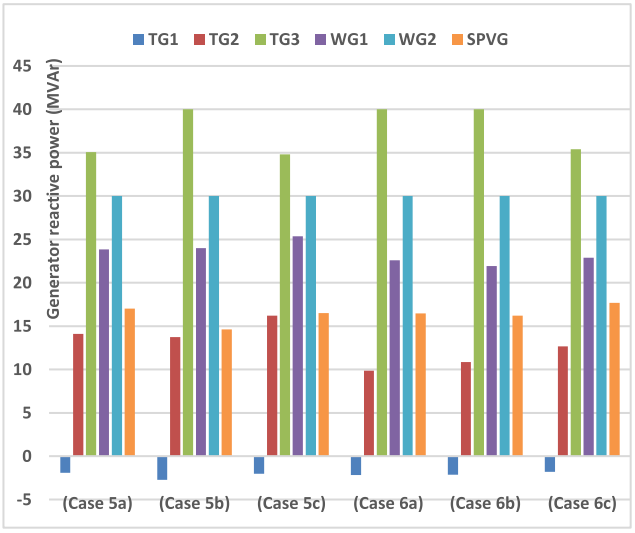

FIGURE 20. Schedule of generator reactive power for case 5 and case 6.

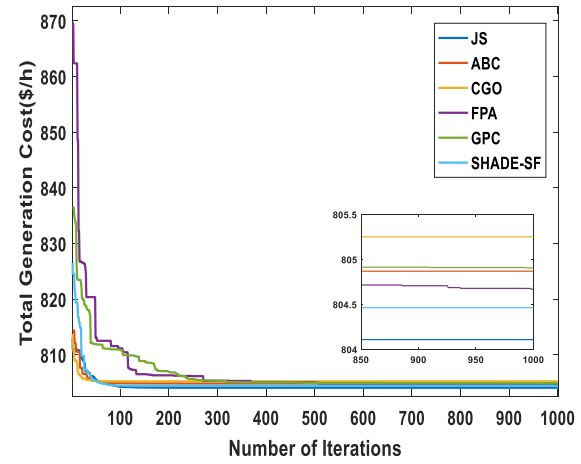

FIGURE 21. Convergence characteristics of different optimization techniques for case-7.

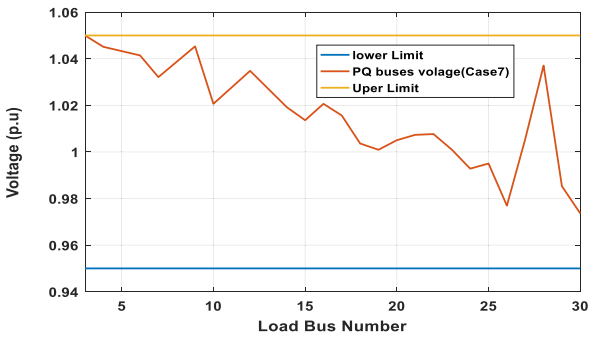

FIGURE 22. Voltage profiles of PQ buses for case-8.

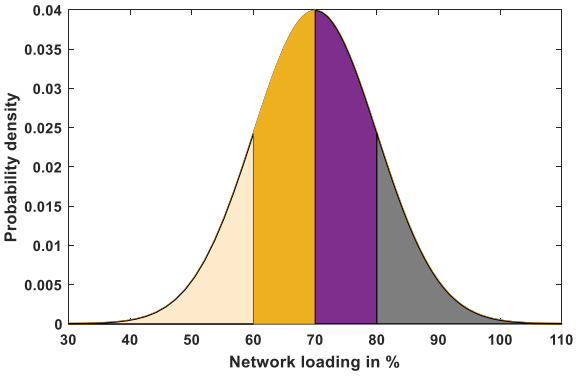

FIGURE 23. Normal distribution representation of load uncertainty with mean $\mu d = 70$, std. dev. $\sigma d = 10$.

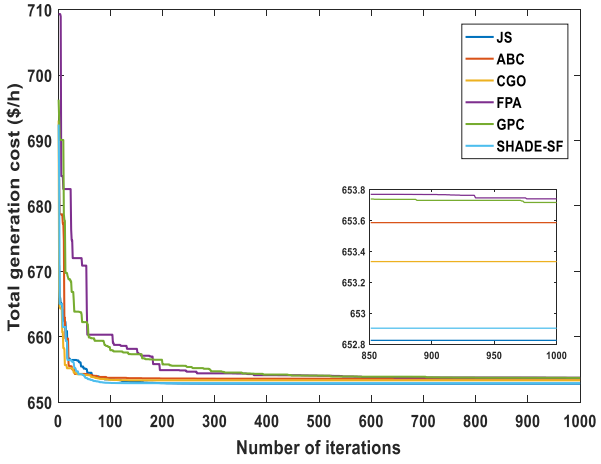

FIGURE 24. Convergence characteristics of different optimization techniques for case-8.

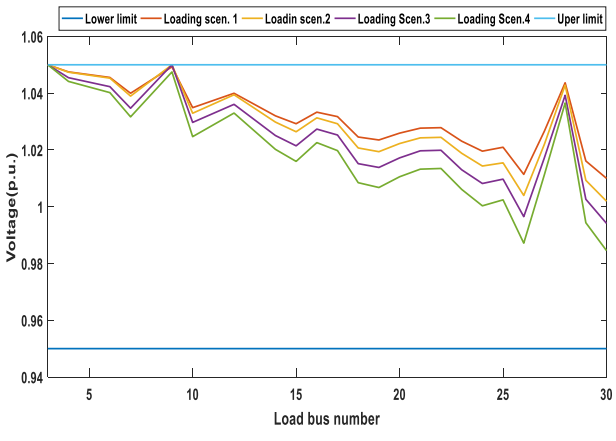

FIGURE 25. Voltage profiles of PQ buses for case-8- for all system loading scenarios.

Table 8 provides the calculated means (as a percentage of nominal loading i.e. 100% of the network loading, P_d) and probabilities for the four loading scenarios. Under each scenario, the six applied algorithms optimize the objective function of total generation cost depending on (11). The scheduled power from all the generators of the system is optimized in each scenario.

Comparing the results given Table 5 (Case 3) and Tables 9-12 (Case 8), it is evident that the network operation cost and power loss are justifiably lower under realistic

loading scenarios. Fig. 24 shows that JS algorithm outperformed all other applied techniques in terms of minimization of total generation cost and solution convergence.

The bus voltage profiles for all the scenarios using JS algorithm are drawn in Fig. 25. The profiles and the state variables listed in Tables 9-12 clearly demonstrate that the JS algorithm duly satisfies all system constraints.

VI. CONCLUSION

In this paper, a new metaheuristic optimization algorithm based on jellyfish search optimizer has been proposed for providing an optimal solution of the OPF problem incorporating with stochastic wind and solar energy sources in the IEEE-30 bus power system. The uncertainty nature of wind and solar energy sources has been modelled with the help of Weibull and lognormal probability density functions (PDFs), respectively. Total generation cost including all generation sources is optimized with and without the imposition of carbon emission tax and the impact of changing cost coefficients of wind and solar energy sources on the generation cost is also studied.

Some practical cases such as the uncertainty of load demand and considering the ramp rate limits of thermal generators have been studied to prove the validity of the proposed algorithm during the practical cases.

To verify the validity of JS algorithm, four recent optimization algorithms: ABC, CGO, FPA, and GPC are applied for the modified IEEE-30 bus system. The simulation results of JS algorithm are compared with the results obtained from the four optimization techniques and the results of another recent optimization algorithm (SHADE-SF) provided in literature.

Simulation results show the effectiveness of the JS algorithm in solving the OPF problem as it exceeds the other optimization algorithms regarding generation cost minimization and solution convergence during the theoretical and practical conditions.

The simulation results of JS and other optimization algorithms show also that the physical and security constraints are within the limits predefined by the system operator.

REFERENCES

[1] J. Carpentier, "Contribution to the economic dispatch problem," *Bull. Soc. Francoise Electriciens*, vol. 8, no. 3, pp. 431–447, 1962.
[2] H. Pourbabak, Q. Alsafasfeh, and W. Su, "Fully distributed AC optimal power flow," *IEEE Access*, vol. 7, pp. 97594–97603, 2019.
[3] P. P. Biswas, P. N. Suganthan, and G. A. J. Amaratunga, "Optimal power flow solutions incorporating stochastic wind and solar power," *Energy Convers. Manage.*, vol. 148, pp. 1194–1207, Sep. 2017.
[4] W. Bai, M. R. Abedi, and K. Y. Lee, "Distributed generation system control strategies with PV and fuel cell in microgrid operation," *Control Eng. Pract.*, vol. 53, pp. 184–193, Aug. 2016.
[5] M. A. Taher, S. Kamel, F. Jurado, and M. Ebeed, "An improved moth-flame optimization algorithm for solving optimal power flow problem," *Int. Trans. Electr. Energy Syst.*, vol. 29, no. 3, p. e2743, Mar. 2019.
[6] K. Y. Lee and A. M. El-Sharkawi, Eds., *Modern Heuristic Optimization Techniques: Theory and Applications to Power Systems*, vol. 39. Hoboken, NJ, USA: Wiley, 2008.
[7] A. Gabash and P. Li, "Active-reactive optimal power flow in distribution networks with embedded generation and battery storage," *IEEE Trans. Power Syst.*, vol. 27, no. 4, pp. 2026–2035, Nov. 2012.
[8] H. Wei, H. Sasaki, J. Kubokawa, and R. Yokoyama, "An interior point nonlinear programming for optimal power flow problems with a novel data structure," *IEEE Trans. Power Syst.*, vol. 13, no. 3, pp. 870–877, Aug. 1998.
[9] S. Frank, I. Steponavice, and S. Rebennack, "Optimal power flow: A bibliographic survey II," *Energy Syst.*, vol. 3, no. 3, pp. 259–289, Sep. 2012, doi: 10.1007/s12667-012-0057-x.
[10] M. R. AlRashidi and M. E. El-Hawary, "Applications of computational intelligence techniques for solving the revived optimal power flow problem," *Electr. Power Syst. Res.*, vol. 79, no. 4, pp. 694–702, Apr. 2009, doi: 10.1016/j.epsr.2008.10.004.
[11] M. A. Abido, "Optimal power flow using tabu search algorithm," *Electr. Power Compon. Syst.*, vol. 30, no. 5, pp. 469–483, 2002.
[12] J. Soares, T. Sousa, H. Morais, Z. Vale, and P. Faria, "An optimal scheduling problem in distribution networks considering V2G," in *Proc. IEEE Symp. Comput. Intell. Appl. Smart Grid (CIASG)*, Apr. 2011, pp. 1–8.
[13] L. L. Lai, J. T. Ma, R. Yokoyama, and M. Zhao, "Improved genetic algorithms for optimal power flow under both normal and contingent operation states," *Int. J. Electr. Power Energy Syst.*, vol. 19, no. 5, pp. 287–292, 1997, doi: 10.1016/s0142-0615(96)00051-8.
[14] M. Younes, M. Rahli, and L. Abdelhakem-Koridak, "Optimal power flow based on hybrid genetic algorithm," *J. Inf. Sci. Eng.*, vol. 23, no. 6, pp. 1801–1816, 2007.
[15] S. R. Paranjothi and K. Anburaja, "Optimal power flow using refined genetic algorithm," *Electr. Power Compon. Syst.*, vol. 30, no. 10, pp. 1055–1063, Oct. 2002, doi: 10.1080/15325000290085343.
[16] H. R. E. H. Bouchekara, A. E. Chaib, and M. A. Abido, "Optimal power flow using GA with a new multi-parent crossover considering: Prohibited zones, valve-point effect, multi-fuels and emission," *Electr. Eng.*, vol. 100, no. 1, pp. 151–165, Mar. 2018, doi: 10.1007/s00202-016-0488-9.
[17] A. G. Bakirtzis, P. N. Biskas, C. E. Zoumas, and V. Petridis, "Optimal power flow by enhanced genetic algorithm," *IEEE Trans. Power Syst.*, vol. 17, no. 2, pp. 229–236, May 2002, doi: 10.1109/TPWRS.2002.1007886.
[18] A. A. El Ela, M. Abido, and S. R. Spea, "Optimal power flow using differential evolution algorithm," *Electr. Eng.*, vol. 80, no. 7, pp. 878–885, Jul. 2010, doi: 10.1016/j.epsr.2009.12.018.
[19] S. Sivasubramani and K. S. Swarup, "Sequential quadratic programming based differential evolution algorithm for optimal power flow problem," *IET Gener., Transmiss. Distrib.*, vol. 5, no. 11, p. 1149, 2011, doi: 10.1049/iet-gtd.2011.0046.
[20] L. Slimani and T. Bouktir, "Optimal power flow solution of the Algerian electrical network using differential evolution algorithm," *TELKOMNIKA Indonesian J. Electr. Eng.*, vol. 10, no. 2, pp. 199–210, Apr. 2012.
[21] S. Sayah and K. Zehar, "Modified differential evolution algorithm for optimal power flow with non-smooth cost functions," *Energy Convers. Manage.*, vol. 49, no. 11, pp. 3036–3042, 2008, doi: 10.1016/j.enconman.2008.06.014.
[22] N. Amjady and H. Sharifzadeh, "Security constrained optimal power flow considering detailed generator model by a new robust differential evolution algorithm," *Electr. Power Syst. Res.*, vol. 81, no. 2, pp. 740–749, Feb. 2011, doi: 10.1016/j.epsr.2010.11.005.
[23] M. A. Abido, "Optimal power flow using particle swarm optimization," *Int. J. Elect. Power Energy Syst.*, vol. 24, no. 7, pp. 563–571, 2002, doi: 10.1016/S0142-0615(01)00067-9.
[24] Q. Kang, M. Zhou, and C. Xu, "Solving optimal power flow problems subject to distributed generator failures via particle swarm intelligence," in *Proc. Int. Conf. Adv. Mechatronics Syst. (ICAMechS)*, 2012, pp. 418–423.
[25] V. H. Hinojosa and R. Araya, "Modeling a mixed-integer-binary small-population evolutionary particle swarm algorithm for solving the optimal power flow problem in electric power systems," *Appl. Soft Comput.*, vol. 13, no. 9, pp. 3839–3852, 2013, doi: 10.1016/j.asoc.2013.05.005.
[26] R.-H. Liang, S.-R. Tsai, Y.-T. Chen, and W.-T. Tseng, "Optimal power flow by a fuzzy based hybrid particle swarm optimization approach," *Electr. Power Syst. Res.*, vol. 81, no. 7, pp. 1466–1474, 2011, doi: 10.1016/j.epsr.2011.02.011.
[27] P. Umapathy, C. Venkataseshaiah, and M. S. Arumugam, "Particle swarm optimization with various inertia weight variants for optimal power flow solution," *Discrete Dyn. Nature Soc.*, vol. 2010, pp. 1–15, Aug. 2010, doi: 10.1155/2010/462145.
[28] H. Tehzeeb-Ul-Hassan, R. Zafar, S. A. Mohsin, and O. Lateef, "Reduction in power transmission loss using fully informed particle swarm optimization," *Int. J. Electr. Power Energy Syst.*, vol. 43, no. 1, pp. 364–368, Dec. 2012, doi: 10.1016/j.ijepes.2012.05.028.

[29] M. Adaryani and A. Karami, "Artificial bee colony algorithm for solving multi-objective optimal power flow problem," *Int. J. Electr. Power Energy Syst.*, vol. 53, pp. 219–230, Dec. 2013.

[30] I. U. Khan, N. Javaid, K. A. A. Gamage, C. J. Taylor, S. Baig, and X. Ma, "Heuristic algorithm based optimal power flow model incorporating stochastic renewable energy sources," *IEEE Access*, vol. 8, pp. 148622–148643, 2020, doi: 10.1109/ACCESS.2020.3015473.

[31] B. Mahdad and K. Srairi, "Security constrained optimal power flow solution using new adaptive partitioning flower pollination algorithm," *Appl. Soft Comput.*, vol. 46, pp. 501–522, Sep. 2016, doi: 10.1016/j.asoc.2016.05.027.

[32] A. E. Hassanien, R. M. Rizk-Allah, and M. Elhoseny, "A hybrid crow search algorithm based on rough searching scheme for solving engineering optimization problems," *J. Ambient Intell. Humanized Comput.*, pp. 1–25, Jun. 2018, doi: 10.1007/s12652-018-0924-y.

[33] N. Daryani, M. T. Hagh, and S. Teimourzadeh, "Adaptive group search optimization algorithm for multi-objective optimal power flow problem," *Appl. Soft Comput.*, vol. 38, pp. 1012–1024, Jan. 2016, doi: 10.1016/j.asoc.2015.10.057.

[34] A. H. Gandomi, X.-S. Yang, and A. H. Alavi, "Cuckoo search algorithm: A metaheuristic approach to solve structural optimization problems," *Eng. Comput.*, vol. 29, no. 1, pp. 17–35, Jan. 2013.

[35] A.-A. A. Mohamed, Y. S. Mohamed, A. A. M. El-Gaafary, and A. M. Hemeida, "Optimal power flow using moth swarm algorithm," *Electr. Power Syst. Res.*, vol. 142, pp. 190–206, Jan. 2017, doi: 10.1016/j.epsr.2016.09.025.

[36] A. Panda and M. Tripathy, "Security constrained optimal power flow solution of wind-thermal generation system using modified bacteria foraging algorithm," *Energy*, vol. 93, pp. 816–827, Dec. 2015, doi: 10.1016/j.energy.2015.09.083.

[37] R. Tanabe and A. Fukunaga, "Success-history based parameter adaptation for differential evolution," in *Proc. IEEE Congr. Evol. Comput.*, Jun. 2013, pp. 71–78.

[38] W. Warid, H. Hizam, N. Mariun, and N. Abdul-Wahab, "Optimal power flow using the Jaya algorithm," *Energies*, vol. 9, no. 9, p. 678, Aug. 2016, doi: 10.3390/en9090678.

[39] F. Berrouk, H. R. E. H. Bouchekara, A. E. Chaib, M. A. Abido, K. Bounaya, and M. S. Javaid, "A new multi-objective Jaya algorithm for solving the optimal power flow problem," *J. Electr. Syst.*, vol. 14, no. 3, pp. 165–181, 2018.

[40] E. E. Elattar and S. K. ElSayed, "Modified Jaya algorithm for optimal power flow incorporating renewable energy sources considering the cost, emission, power loss and voltage profile improvement," *Energy*, vol. 178, pp. 598–609, Dec. 2018.

[41] W. Gao, S. Liu, and L. Huang, "A global best artificial bee colony algorithm for global optimization," *J. Comput. Appl. Math.*, vol. 236, no. 11, pp. 2741–2753, 2012.

[42] P. P. Biswas, P. N. Suganthan, and G. A. J. Amaratunga, "Optimal power flow solutions incorporating stochastic wind and solar power," *Energy Convers. Manage.*, vol. 148, pp. 1194–1207, Sep. 2017.

[43] J.-S. Chou and D.-N. Truong, "A novel metaheuristic optimizer inspired by behavior of jellyfish in ocean," *Appl. Math. Comput.*, vol. 389, Jan. 2021, Art. no. 125535.

[44] S. Harifi, J. Mohammadzadeh, M. Khalilian, and S. Ebrahimnejad, "Giza pyramids construction: An ancient-inspired metaheuristic algorithm for optimization," *Evol. Intell.*, pp. 1–9, Jul. 2020, doi: 10.1007/s12065-020-00451-3.

[45] S. Talatahari and M. Azizi, "Chaos game optimization: A novel metaheuristic algorithm," *Artif. Intell. Rev.*, vol. 54, pp. 917–1004, 2021, doi: 10.1007/s10462-020-09867-w.

[46] X. S. Yang, "Flower pollination algorithm for global optimization," in *Unconventional Computation and Natural Computation* (Lecture Notes in Computer Science), vol. 7445, J. Durand-Lose and N. Jonoska, Eds. Berlin, Germany: Springer, 2012, pp. 240–249, doi: 10.1007/978-3-642-32894-7_27.

[47] O. Alsac and B. Stott, "Optimal load flow with steady-state security," *IEEE Trans. Power App. Syst.*, vol. PAS-3, no. 3, pp. 745–751, May 1974.

[48] A. E. Chaib, H. R. E. H. Bouchekara, R. Mehasni, and M. A. Abido, "Optimal power flow with emission and non-smooth cost functions using backtracking search optimization algorithm," *Int. J. Elect. Power Energy Syst.*, vol. 81, pp. 64–77, Oct. 2016.

[49] L. Shi, C. Wang, L. Yao, Y. Ni, and M. Bazargan, "Optimal power flow solution incorporating wind power," *IEEE Syst. J.*, vol. 6, no. 2, pp. 233–241, Jun. 2012.

[50] C. Tian-Pau, "Investigation on frequency distribution of global radiation using different probability density functions," *Int. J. Appl. Sci. Eng.*, vol. 8, no. 2, pp. 99–107, 2010.

[51] F. Yao, Z. Y. Dong, K. Meng, Z. Xu, H. H.-C. Iu, and K. P. Wong, "Quantum-inspired particle swarm optimization for power system operations considering wind power uncertainty and carbon tax in Australia," *IEEE Trans. Ind. Informat.*, vol. 8, no. 4, pp. 880–888, Nov. 2012.

[52] T. Ackermann, *Wind Power in Power System*. Hoboken, NJ, USA: Wiley, 2012, ch. 43.

[53] S. Eftekharnejad, V. Vittal, Heydt, B. Keel, and J. Loehr, "Impact of increased penetration of photovoltaic generation on power systems," *IEEE Trans. Power Syst.*, vol. 28, no. 2, pp. 893–901, May 2013.

[54] R. Albarracín and M. Alonso, "Photovoltaic reactive power limits," in *Proc. 12th Int. Conf. Environ. Electr. Eng.*, May 2013, pp. 13–18.

[55] A. Cabrera-Tobar, E. Bullich-Massagué, M. Aragues-Penalba, and O. Gomis-Bellmunt, "Reactive power capability analysis of a photovoltaic generator for large scale power plants," in *Proc. 5th IET Int. Conf. Renew. Power Gener.*, 2016, pp. 53–56.

[56] *Wind Turbines Part1: Design Requirements*, Standard IEC 61400-1, International Electrotechnical Commission, 2005.

[57] S. S. Reddy, P. R. Bijwe, and A. R. Abhyankar, "Real-time economic dispatch considering renewable power generation variability and uncertainty over scheduling period," *IEEE Syst. J.*, vol. 9, no. 4, pp. 1440–1451, Dec. 2015.

[58] H. M. Dubey, M. Pandit, and B. K. Panigrahi, "Hybrid flower pollination algorithm with time-varying fuzzy selection mechanism for wind integrated multi-objective dynamic economic dispatch," *Renew. Energy*, vol. 83, pp. 188–202, Nov. 2015.

[59] J. M. Morales, A. J. Conejo, K. Liu, and J. Zhong, "Pricing electricity in pools with wind producers," *IEEE Trans. Power Syst.*, vol. 27, no. 3, pp. 1366–1376, Aug. 2012.

[60] B. Veatch, "Cost and performance data for power generation technologies," BVH Company, Lincoln, NE, USA, Tech. Rep., Feb. 2012, pp. 1–109.

[61] T. Niknam, M. R. Narimani, J. Aghaei, S. Tabatabaei, and M. Nayeripour, "Modified honey bee mating optimisation to solve dynamic optimal power flow considering generator constraints," *IET Gener., Transmiss. Distrib.*, vol. 5, no. 10, p. 989, 2011.

[62] S. M. Mohseni-Bonab, A. Rabiee, and B. Mohammadi-Ivatloo, "Voltage stability constrained multi-objective optimal reactive power dispatch under load and wind power uncertainties: A stochastic approach," *Renew. Energy*, vol. 85, pp. 598–609, Jan. 2016, doi: 10.1016/j.renene.2015.07.021.

[63] P. P. Biswas, P. Arora, R. Mallipeddi, P. N. Suganthan, and B. K. Panigrahi, "Optimal placement and sizing of FACTS devices for optimal power flow in a wind power integrated electrical network," *Neural Comput. Appl.*, vol. 33, no. 12, pp. 6753–6774, Jun. 2021, doi: 10.1007/s00521-020-05453-x.